12-2017

Remediation of Lead and Copper Ions from Water Solutions Using Transition Metal Sulfides

Jesus M. Cantu Jr.
The University of Texas Rio Grande Valley

REMEDIATION OF LEAD AND COPPER IONS FROM WATER SOLUTIONS USING TRANSITION METAL SULFIDES

A Thesis

by

JESUS M. CANTU JR.

Submitted to the Graduate College of
The University of Texas Rio Grande Valley
In partial fulfillment of the requirements for the degree of

MASTER OF SCIENCE

December 2017

Major Subject: Chemistry

REMEDIATION OF LEAD AND COPPER IONS FROM AQUEOUS SOLUTIONS USING TRANSITION METAL SULFIDES

A Thesis
by
JESUS M. CANTU JR.

COMMITTEE MEMBERS

Dr. Jason G. Parsons
Chair of Committee

Dr. Evangelia Kotsikorou
Committee Member

Dr. Jose J. Gutierrez
Committee Member

Dr. Justin Moore
Committee Member

December 2017

ABSTRACT

Cantu, Jesus M. Jr., Remediation of Lead and Copper Ions from Aqueous Solutions Using Transition Metal Sulfides. Master of Science (MS), December, 2017. 56 pp., 10 tables, 25 figures, references, 37 titles.

Heavy metal contamination in water solutions has been a major concern since many transition metals don't play a role in any biological function and are actually detrimental to human health. There have been several techniques that have been implemented for the remediation of heavy metal contaminants. For this project, three metal sulfides—Fe_7S_8, ZnS, TiS_2—were synthesized and studied for their capabilities to remove Pb(II) and Cu(II) from water solutions. Several parameters were investigated to determine the effects of pH, time, temperature, binding capacities, and interfering ions. The room temperature adsorption capacities ranged 6.23-333.3 mg/g for Pb(II) and 1.31-250 mg/g for Cu(II). The thermodynamic parameters determined that the process for the binding of Pb(II) to Fe_7S_8, ZnS (absence of light), and TiS_2 was spontaneous whereas the binding with ZnS in ambient light was non-spontaneous. On the other hand, the binding of Cu(II) to Fe_7S_8 and ZnS was non-spontaneous but for TiS_2 the reaction was spontaneous.

DEDICATION

This thesis is dedicated to my parents, Jesus Cantu and Alma Cantu, who have always been there for me. They have worked very hard to ensure that I succeed in life, and have taught me that I can accomplish anything I put my mind to.

I also dedicate this thesis to my sister, Yvette Cantu, whose guidance has helped me throughout all my life. Without her wisdom and support, I would not have been able to accomplish this work.

Finally, I would like dedicate this work to my brother, Victor Cantu, who has taught me to enjoy life and have fun even when its most stressing. He has always been there to take my mind off of school work.

ACKNOWLEDGMENTS

I would like to begin by thanking my advisor, Dr. Jason G. Parsons, for giving me the opportunity to work in his lab. Under his guidance, not only did I gain experience in various fields of chemistry, but I got the got the chance to present my work in several conferences, for which I am very grateful. I would like to also thank him for encouraging me to pursue a Ph.D. in chemistry. I would like to further express my gratitude to him for his knowledge, dedication, and patience with me for which without it, this work wouldn't have been possible. I would like to thank my committee members: Dr. Evangelia Kotsikorou, Dr. Jose J. Gutierrez, and Dr. Justin H. Moore for their knowledge and expertise.

I would like to thank Thomas Eubanks for his assistance with instrumentation. I would also like to thank Ale Carvajal for her assistance with conference trips.

I would like to thank the past and present lab colleagues including Carolina Valdes, Diego F. Gonzalez, John Paul Valle, Kenneth Flores, Yvette Cantu, and Jacob Sollner for all their help with the experiments and all the fun times we had in lab.

TABLE OF CONTENTS

Page

LIST OF TABLES

Page

LIST OF FIGURES

Page

CHAPTER I

INTRODUCTION

Heavy Metal Contamination of Water Systems

The earth is approximately three-fourths water of which only 2.5-2.75% is fresh water. From the fresh water only 1.2% is surface water, whereas the rest of the water is distributed between ground water and glaciers which contain the majority of the fresh water[1]. With small percentage of potable water, contamination due to industrialization has become a global concern for both environment and human health. Such contamination can be divided in to two general chemical classes organic and inorganic pollutants, which include chemical compounds such as pesticides, detergents, fertilizers, acid wastes, and heavy metal ions. More specifically, lead and copper have received a lot of interest due to the health-related issues upon exposure. Copper is commonly used industrially for pipes, valves, alloys and coatings. Furthermore, it has also been used as an algaecide added to surface water in order to diminish algae growth [3]. On the other hand, lead has been commonly used in lead-acid batteries, solder, alloys, in the organometallic form, tetraethyl and tetramethyl. lead has been used as lubricating and anti-knocking agents [3]. Interestingly, lead is not normally found in tap water; however, lead has been found an enters drinking water from lead containing household plumbing systems such as: pipes and fittings [3]. With water running through lead contacting plumbing system, the lead can dissolve and can be consumed. The amount of dissolved lead in the water is dependent on the pH, water hardness, temperature, and contact time [3]. The environmental Protection Agency (EPA), a government

agency that regulates the potential environmental pollutants. The EPA in correspondence to the Safe Drinking Water Act (SDWA), have set maximum contaminant levels (MCLs) for copper and lead at 1.3 mg/L (ppm) and 0.015 mg/L, respectively [4].

Since lead does not have a biological role in the human body, the health-related issues upon exposure are numerous. Lead exposure has been linked to a number of health problems such as: disruption of the nervous system, disruption of the renal system, and disruption in the production of hemoglobin. These heat related issues occur since lead is a divalent cation that strongly binds to proteins with sulfur groups. Furthermore, lead competes with the uptake of calcium. For instance, at low concentrations, it binds to phosphokinase C, which competes with calcium and affects neuron signaling [5]. The toxicity of lead is more of a concern with respect to children which can absorb 4-5 times more lead than adults [6, 7]. In adults, lead generally affects the kidneys, blood pressure, and the nervous system (peripheral and central nervous systems) [5].

On the other hand, copper is a trace essential element for humans and is therefore needed in low concentrations for biological purposes. For example, copper is commonly found in enzymes such as: tyrosinase, p-hydroxyphenyl pyruvate hydrolase, and cytochrome c oxidase [2]. The consumption of high amounts of copper, in the early stages, can trigger anorexia and lethargy [2]. Furthermore, ingestion of high concentrations of copper are toxic to the body and can lead to liver toxicity, which can further cause lesions to the central nervous systems, abdominal pain and diarrhea [8-10].

Current Heavy Metal Remediation Methods

Industrial processes tend to produce large amounts of waste consisting of either organic waste or inorganic waste. Some examples of industrial processes that produce either lead or copper waste are: battery manufacturing, electroplating, fertilizer industry, paint manufacturing, metal smelting, mining, and oil refining processes [10-12]. The disposal of contaminated waste has been shown to contaminate water systems since these ions are not degraded like organic waste and tend to be persistent in the environment. Therefore, removal of heavy metal contaminants from potable water has become a major concern globally. Over the past few decades, remediation techniques have been developed and used for the removal of heavy metal ions from water systems. Current techniques for the removal of lead and copper include but are not limited to: ion-exchange, biosorption, precipitation, and adsorption [13]. Ion-exchange involves the use of an ion exchange solid—usually an organic resin—to exchange cations or anions from the water with protons (H^+) or hydroxide ions (OH^-) ions found in the resin [13]. Biosorption is similar to adsorption, however, it uses a biomass material such as pine wood, algae, sawdust, pomegranate peel, alfalfa biomass to remove contaminants form water. Precipitation treatment for the removal of heavy metal contaminants from water involves the use of chemical precipitants, coagulants, and flocculants to complex the contaminants and remove them via precipitation [13]. Although the afore mentioned techniques have proven to be effective in the removal of heavy metal ions, they have several disadvantages to their usage such as: complicated to implement, high cost, and low removal capacities. Furthermore, each technique has its own disadvantage, which has to be considered before implementation. For example, precipitation requires precipitating agents that normally generate sludge which then has to be removed prior to further treatment. Ion exchange processes generally are not specific towards the ion being removed all cations or anions react

with the resins. However, adsorption has shown much promise for the removal of heavy metal ions from water. Furthermore, the use of nano-sized adsorbents, which have high surface area and high reactivity have shown great promise as a remediation/ cleaning technology. The ease of implementation, high capacities for removal, and cost effectiveness have attracted a lot of attention, recently.

Several adsorbents have been studied for their capabilities to remove heavy metal ions from water systems. For example, iron oxides, iron sulfides, aluminum oxides, graphene oxides, zinc oxides, copper oxides, sawdust, biochar, biosorbents, titanium dioxide, red mud, activated carbon, granular ferric oxides (GFO's), and among other types of materials have been investigated[8-18]. Although there are several adsorbents showing promising results in the binding of heavy metal ions, iron-based particles are of interest due to their magnetic properties. For instance, the use of Fe_2O_3 and Fe_3O_4 exhibited favorable results in the adsorption of both Cu(II) and Pb(II) from aqueous solutions. Tamez et al. found that Fe_2O_3 exhibited a binding capacity of 47.62 mg/g and 19.61 mg/g for Pb(II) and Cu(II), respectively, while Fe_3O_4 showed binding capacities of 166.67 mg/g and 37.04 mg/g for Pb(II) and Cu(II), respectively [10]. Additionally, Sitko et al. found graphene oxide have capacities up to 1119 mg/g and 294 mg/g for Pb(II) and Cu(II), respectively [15].

Proposed Adsorbent Nanomaterials

In the present study, transition metal sulfides (Fe_7S_8, ZnS, TiS_2) were of interest for the removal of lead and copper. Similar to the synthesis of many transition metal oxides, the synthesis of transition metal sulfide nanomaterials is inexpensive and relatively simple. The focus of the present study was to conduct a facile, inexpensive synthesis of transition metal sulfide based adsorbents. Furthermore, to test the capabilities of Fe_7S_8, ZnS, TiS_2 in the removal of lead and copper from aqueous solutions. Several batch studies were performed to determine the effects of pH, temperature, the binding kinetics, thermodynamics of binding, and binding capacity of the nanoparticles of transition metal sulfide. In addition, batch interference studies were performed to simulate natural water systems by incorporating common hard cations and test their effect on the binding process.

CHAPTER II

MATERIALS AND METHODS

Synthesis of Transition Metal Sulfides

Synthesis of Fe_7S_8 Nanomaterial

Pyrrhotite (Fe_7S_8) nanomaterial was synthesized using a method similar to that used by Cantu et al [20]. The synthesis involved the dissolution of 60 mmol of thiourea and 30 mmol iron (III) chloride hexahydrate ($FeCl_3$ 6 H_2O) in a mixture of 60 mL ethylene glycol and 20 mL of ultra-pure water (18 Ω). The mixture was then transferred to Teflon lined autoclaves filled to approximately 80% of the capacity. The autoclaves were then sealed and reacted at 180˚C for 1 hr. Subsequent to the reaction, the autoclaves were allowed to cool to room temperature naturally and the products were vacuum filtered using a Buchner funnel. The products were washed with methanol and acetone to remove any unreacted starting materials and byproducts formed during the reaction.

Synthesis of ZnS Nanomaterial

The zinc sulfide nanomaterial (ZnS) was synthesized via a hydrothermal method similar to that used by Hoa et al [21]. For the synthesis, 60 mmol of zinc nitrate hexahydrate ($Zn(NO_3)_2$ 6 H_2O) and 60 mmol of sodium sulfide nonahydrate (Na_2S $9H_2O$) were dissolved in 60 mL of ultra-pure water, separately. Then the sodium sulfide solution was added to the zinc nitrate solution dropwise while stirring. After the addition of the reagent the mixture was transferred

into Teflon lined autoclaves were filled to approximately 80% of their capacity and reacted at 150˚C for 3h. After the reaction, the autoclaves were cooled to room temperature naturally and the product was then transferred to clean 50 mL conical vials and centrifuged at 3500 rpm for 5 min. The supernatant was decanted and the product was washed three times using ultra-pure water. Finally, the sample was allowed to air dry overnight at room temperature.

Synthesis of TiS_2 Nanomaterial

The titanium (IV) sulfide (TiS_2) was synthesized using a as a previously described synthesis method describe by Prabakar et al.[22]. In the synthesis, 120 mmol of elemental sulfur was added to 250 mL of 1-octadecene. The flask was purged with argon gas and heated to 300˚C. Once the reaction mixture reached temperature, 20 mmol of titanium tetrachloride ($TiCl_4$) was injected and the solution was refluxed for 30 min. Subsequent to reaction, the product was cooled to room temperature. The black precipitate was then vacuum filtered and washed using a combination of methanol, toluene, and acetone to remove the any residual organic solvent and any byproducts that may have formed during the reaction.

X-Ray Diffraction (XRD) Analysis

All nanomaterials were characterized using x-ray diffraction; each analysis was performed using a Rigaku Miniflex Diffractometer. The products were homogenized using a mortar and pestle into fine powders. The XRD patterns were collected from 20˚ to 60˚ for both Fe_7S_8 and ZnS; however, the TiS_2 diffraction pattern was collected from 10˚ to 70˚. All diffraction patterns were collected with a step width of 0.05˚ in 2θ and a counting time of 5 s. In addition, the patterns were collected using a Cu source (K_α=1.541 Å) with a nickel filter. From

the XRD patterns, the average particle size was determined using a Gaussian fitting and Scherrer's equation. In addition, each powder XRD pattern was fitted using t the Fullprof 2001 Suite of programs and crystallographic data from the literature [20].

Determination of Optimum Binding pH

The effect of the pH on the binding of Pb(II) and Cu(II) to the Fe_7S_8, ZnS, and TiS_2 was studied by preparing 0.3 mM and 0.3 ppm (mg/L) solutions, respectively. The pH of the solutions was adjusted to pH's 2, 3, 4, 5, and 6 using either dilute nitric acid (HNO_3) or dilute sodium hydroxide (NaOH). For the reactions, 4.0 mL aliquots of each pH-adjusted solution were transferred into reaction sample test tubes containing 10 mg of either Fe_7S_8, ZnS, or TiS_2 nanomaterial. Additional 4.0 mL aliquots were pipetted into empty test tubes to serve as controls for the reaction. The reactions and controls were performed in triplicate for statistical purposes. The test tubes were then equilibrated on a rocker for 1h at room temperature. After equilibration, the sample and control tubes were centrifuged at 3500 rpm for 5 min, and the supernatants were decanted and stored for further analysis via ICP-OES.

UV-Light pH studies for the ZnS Nanomaterial

The effect of the presence of UV-light was studied for the binding of Pb(II) and Cu(II) to the ZnS nanomaterial due to the photo absorption properties of the ZnS nanomaterial. For the reaction, 100 ppm solutions of Pb(II) and Cu(II) were prepared and the solutions were pH-adjusted to pH's 2, 3, 4, 5, and 6 using either dilute nitric acid (HNO_3) or dilute sodium hydroxide (NaOH). For the reactions, 8.0 mL aliquots of each pH-adjusted solution were transferred into 50 mL beakers containing 20 mg of ZnS. In addition, control samples which

consisted of the 8.0 mL aliquot of the pH adjusted metal solution in the absence of the nanomaterial. The reactions and control samples were performed in triplicate for statistical purposes. The beakers were equilibrated in a Innova44 incubator using a mercury lamp illumination for 1h. Subsequent to reaction, the samples were transferred into test tubes and centrifuged at 3500 rpm for 5 min. The supernatants were decanted and stored in clean test tubes for further analysis using ICP-OES. All other studies were conducted under UV-light instead of ambient light.

Dark pH studies of the ZnS nanomaterial

The effect of the absence of light on the binding of Pb(II) and Cu(II) was investigated. For the reaction, 100 ppm solutions of Pb(II) and Cu(II) were prepared and the solutions were pH-adjusted to pH's 2, 3, 4, 5, and 6 using either dilute HNO_3 or dilute NaOH. For the reactions, 4.0 mL aliquots of each pH-adjusted solution were transferred into clean 5 mL tubes containing 10 mg of ZnS. The controls for the reaction consisted of 4.0 mL aliquots of the pH adjusted metal solution in the absence of the nanomaterial. The reaction and control samples were performed in triplicate for statistical purposes. The reactions were equilibrated on a rocker in the dark for 1 h. Subsequent to reaction, the reaction and control tubes were centrifuged at 3500 rpm for 5 min and the supernatants were decanted and stored for further analysis using ICP-OES. All other studies were conducted as a dark box instead of ambient light.

Kinetic Studies

The required time for the reaction was determined for the adsorption of Cu(II) and Pb(II) to each nanomaterial. For the process, the concentrations of the Pb(II) and Cu(II) solutions varied

between each transition metal sulfide nanomaterial which were made using Millipore (18Ω) water and pH adjusted to the respective optimum binding pH. The pH adjustment was performed as previously mentioned.

- Fe_7S_8—Concentrations of 0.3 mM Pb(II) and 30 ppm Cu(II).
- ZnS (ambient light)—Concentrations of 0.3 mM Pb(II) and 30 ppm Cu(II).
- ZnS (absence of light)—Concentration of 100 ppm Pb(II).
- TiS_2—Concentrations of 1000 ppm Pb(II) and Cu(II).

4.0 mL aliquots of the pH adjusted solution was transferred to clean 5 mL test tubes containing 10 mg of either Fe_7S_8, ZnS, or TiS_2 and into control test tubes. The reaction and controls were equilibrated on a rocker for 5, 10, 15, 30, 60, 90, 120, and 240 min. In addition, the reactions were performed at three temperatures 4˚C, 22˚C and 45˚C. The reaction and control samples were performed in triplicate for statistical purposes. Subsequent to equilibration for their respective time, the samples and controls were centrifuged at 3500 rpm and the supernatant was decanted and stored for further analysis using ICP-OES.

Capacity Studies for Nanomaterials

The binding capacity of each nanomaterial was determined by binding various concentrations of either Pb(II) and Cu(II) to the nanomaterial. The concentrations of Pb(II) and Cu(II) prepared for Fe_7S_8, ZnS (dark), TiS_2 were 0.3, 3, 30, 100, 300, and 1000 ppm whereas the concentrations for ZnS (ambient light) were 800, 1200, 1500, 2000, and 3000 ppm for both ions. The solutions were pH-adjusted to each nanomaterial's optimum pH. 4.0 mL aliquots of the pH adjusted metal solutions were the transferred to 5 mL tubes containing 10 mg of either Fe_7S_8, ZnS, or TiS_2. In addition, 4.0 mL aliquots were pipetted into control tubes, which did not contain

the nanomaterial. The reaction and control samples were replicated in triplicate for statistical purposes. The reaction and control tubes were equilibrated on a rocker for 1h. Subsequent to the reaction, the sample and control tubes were centrifuged at 3500 rpm for 5 min. The supernatants were then decanted and stored for further analysis using ICP-OES.

Thermodynamic Studies

The thermodynamics for the adsorption process were performed in conjunction with the capacity studies to determine the thermodynamic parameters for the reactions: ΔG, ΔS, and ΔH. The concentrations of either Cu(II) and Pb(II) for binding with Fe_7S_8, ZnS (absence of light), TiS_2 were 0.3, 3, 30, 100, 300, and 1000 ppm. Whereas the concentrations for ZnS (ambient light) were 800, 1200, 1500, 2000, and 3000 ppm for both ions. After pH-adjustment of each metal solution for the respective nanomaterial, 4.0 mL aliquots were transferred into clean 5 mL tubes containing 10 mg of either Fe_7S_8, ZnS, or TiS_2. In addition, control tubes which did not contain any nanomaterial were also set up. The tubes were equilibrated on rockers at three different temperatures 4˚C, 22˚C, and 45˚C for 1h. The reaction and control samples were performed in triplicate for statistical purposes. After equilibration, the sample and control tubes were centrifuged at 3500 rpm for 5 min and the supernatants were decanted stored for further analysis using ICP-OES.

Binding Interference Studies

The binding of Pb(II) and Cu(II) ions were tested with the presence of commonly found cations present in water systems as possible interferences on the binding process. The cations tested were Na^+, K^+, Mg^{2+}, and Ca^{2+}. The cations were added to the 0.3 mM Pb(II) and 0.3 ppm

Cu(II) solutions concentrations of 0.3, 3, 30, 100, 300, and 1000 ppm, and the solutions were pH adjusted to each nanomaterial's optimum pH, as previously mentioned. Aliquots of 4.0 mL were transferred into clean 5 mL test tubes containing 10 mg of either Fe_7S_8, ZnS, or TiS_2. Control samples which consisted of 4.0 mL aliquots of the pH adjusted metal solution in the absence of the nanomaterial. Furthermore, the reactions were performed in triplicate for statistical purposes. The solutions were then equilibrated on a rocker for 1h and the sample test tubes were centrifuged at 3500 rpm for 5 min. The supernatants were decanted and stored for further analysis using ICP-OES.

ICP-OES Parameters

The ICP-OES analysis was performed using a Perkin Elmer Optima 8300 ICP-OES (Perkin Elmer, Shelton CT) with Winlab32 software. The parameters for the analysis are shown in Table 1. Samples that were too concentrated were diluted to fall within values used for the calibration of the instrument. The results for Pb(II) and Cu(II) for each analysis were obtained using calibration curves with correlation coefficients (R^2) of 0.99 or better.

Table 1: ICP-OES parameters used for the analysis of Pb(II) and Cu(II) solutions after reaction with the nano-metal sulfide nanomaterials.

Parameter	Setting
λ_{Pb}	217.0 nm
λ_{Cu}	327.393 nm
RF power	1500 W
Nebulizer	Gemcone (low flow)
Plasma Flow	15 L/min
Auxiliary Flow	0.2 L/min
Nebulizer Flow	0.55 L/min
Sample Flow	1.50 mL/min
Injector	2.0 mm Alumina
Spray Chamber	Cyclonic
Integration Time	20 seconds
Replicates	3

CHAPTER III

RESULTS AND DISCUSSION

Structures and properties

The geometry of the iron sulfide (Fe_7S_8) nanomaterial was monoclinic with a space group C 2 / C and lattice parameters of a = 12.00185 Å, b = 6.88428 Å, and c = 13.18790 Å. The geometry of the zinc sulfide nanomaterial is cubic with a space group of F 43 M and lattice parameters of a = b = c = 5.406310 Å. ZnS was of interest due to its photo-catalytic properties. The titanium (IV) sulfide (TiS_2) nanomaterial has a trigonal geometry with a space group P 3 M 1 and lattice parameters of a = b = 3.397 Å and c = 5.747 Å. It consists of an anisotropic layered structure in which the its layered where the stacking occurs along the c-axis and is separated by gaps.

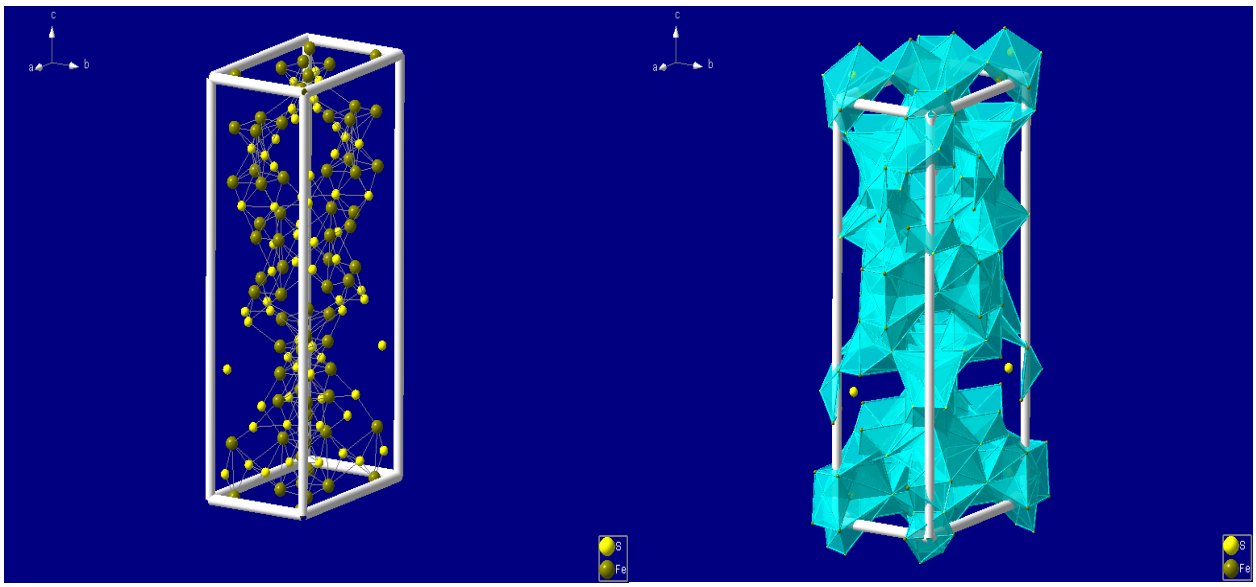

Figure 1: Fe_7S_8 crystal structure

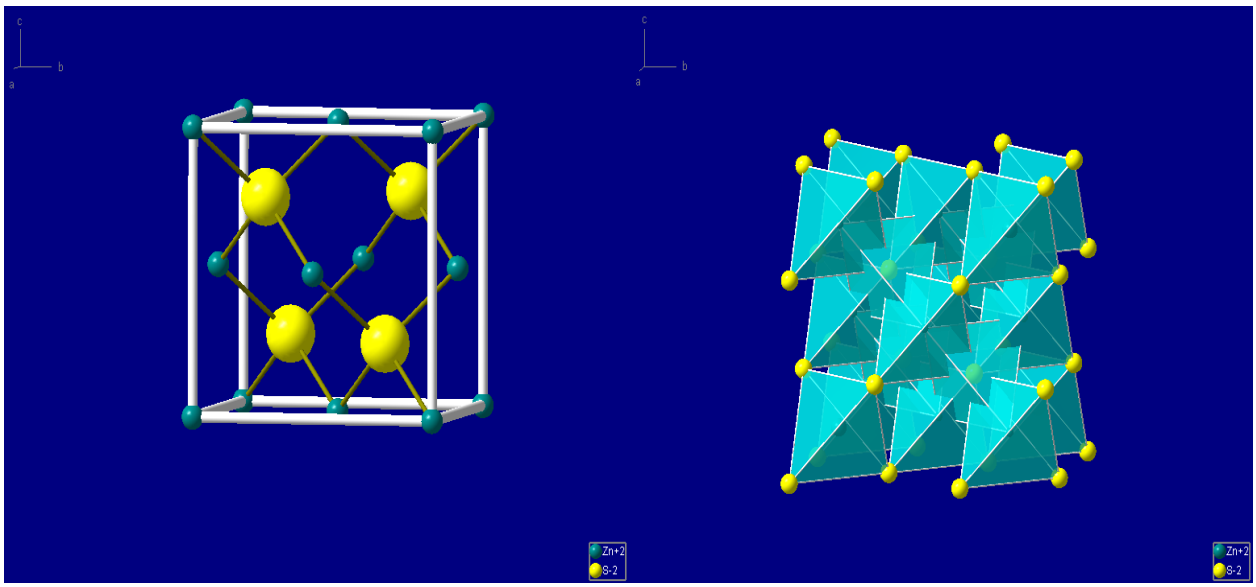

Figure 2: ZnS crystal structure

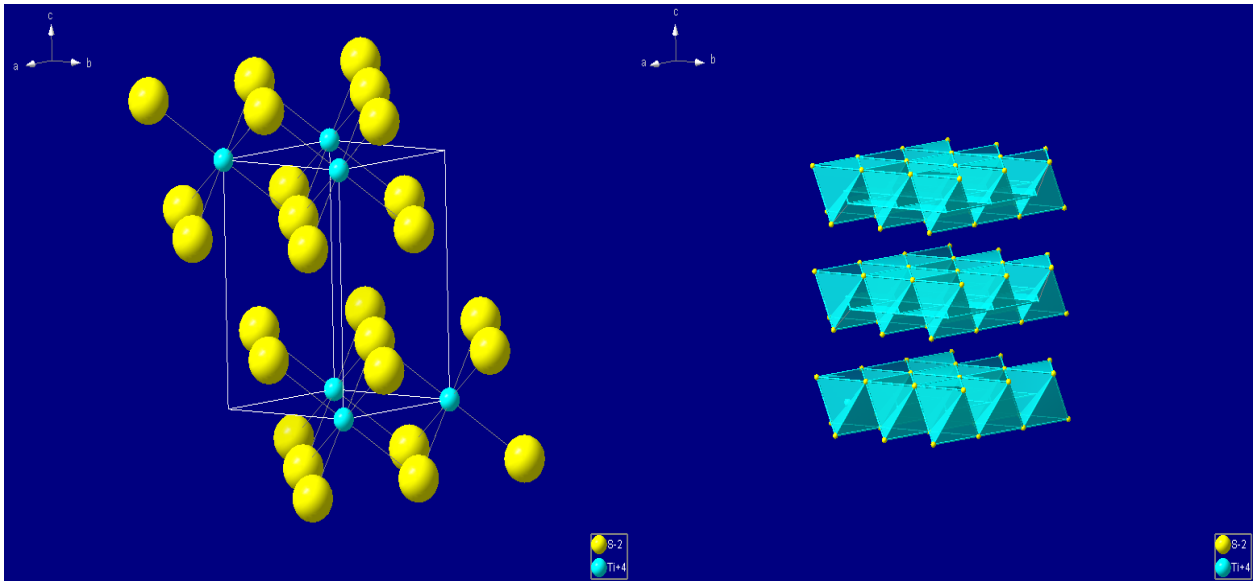

Figure 3: TiS_2 crystal structure

Nanomaterial Characterization

The X-ray diffraction patterns for the synthesized nanomaterials are shown in Figures 4-6. Figure 4 shows the diffraction pattern for Fe_7S_8. From the pattern, it was determined that the material consisted of two phases: Fe_7S_8 (pyrrhotite) and Fe_3S_4 (greigite). The majority of the material was Fe_7S_8, which was approximately 90% of the sample and the remaining 10% was the Fe_3S_4 phase. Due to the composition of the sample, the biding occurring in the sample was assumed to be due to the Fe_7S_8 phase. The space group of the Fe_7S_8 phase was determined to be monoclinic C2/C with lattice parameters of: a=12.00185 Å, b=6.88428 Å, and c=13.18790 Å with $\alpha=\gamma=90^\circ$ and $\beta=119.419^\circ$, which correspond to the literature values [23]. On the other hand, the space group for the Fe_3S_4 phase was determined to be cubic FD3M with lattice parameters of: a=b=c=9.96841 Å with $\alpha=\beta=\gamma=90^\circ$, which also corresponded to the literature values [24]. Furthermore, the average particle size for the synthesized Fe_7S_8 was calculated to be 23.3 nm based on the 023 diffraction peak occurring at (35.04˚) and the average particle size for the greigite phase was calculated to be 18.7 nm based on the 400 peak occurring at (36.04˚).

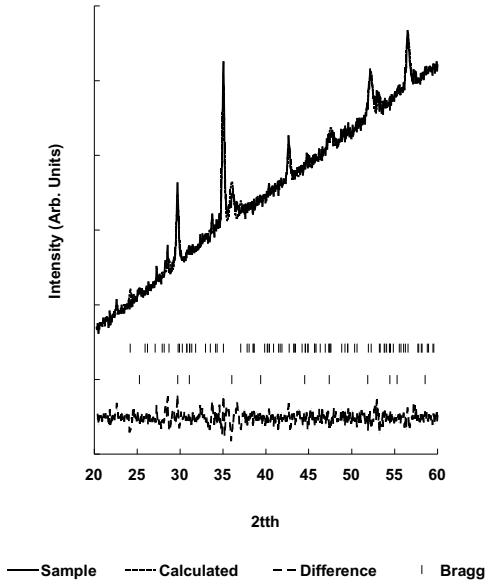

Figure 4: Powder x-ray diffraction pattern collected for the synthesized iron sulfide nanomaterial

The diffraction pattern for the ZnS is shown in Figure 5. From the pattern, it was determined that the ZnS was in cubic crystal structure in the F43M space group with the following lattice parameters: a=b=c= 5.406310 Å and α=β=γ=90˚, which are in correspondence to the literature values [25]. Furthermore, the average particle size was calculated to be 7.0 ± 0.22 nm based on the average size calculated from the three most prominent diffraction peaks.

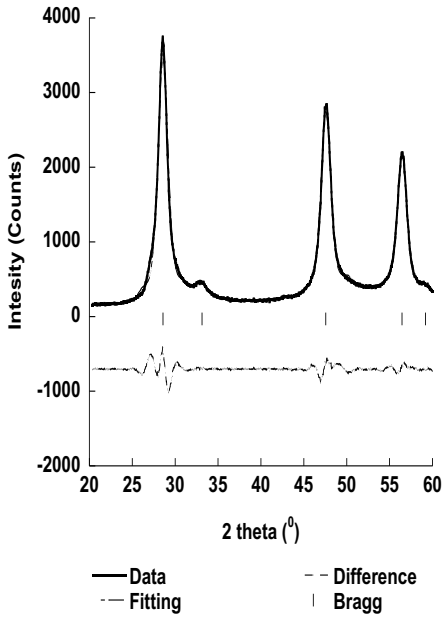

Figure 5: Powder x-ray diffraction pattern collected for the synthesized zinc sulfide nanomaterial

The x-ray diffraction pattern for the TiS_2 nanomaterial is shown in Figure 6. It was determined that the synthesized TiS_2 was in a trigonal crystal structure with a space group of P3M1. The refine lattice parameters were determined to be a=b=3.397 Å and c=5.747 Å with $\alpha=\beta=90^{\circ}$ and $\gamma=120^{\circ}$. Additionally, the average particle size for the synthesized titanium disulfide was calculated to be 8.03 ± 0.98 nm. The lattice parameters for each nanomaterial are shown in Table 2.

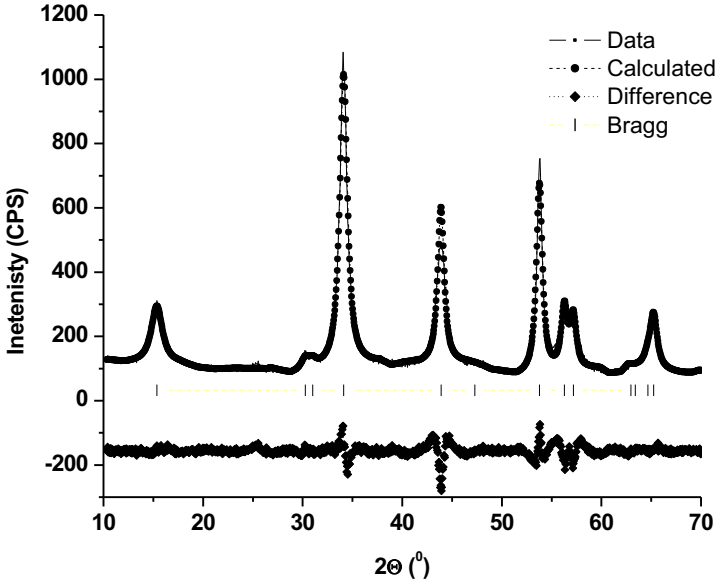

Figure 6: Powder x-ray diffraction pattern collected for the synthesized titanium disulfide nanomaterial

Table 2: Fitting parameters for the synthesized transition metal sulfides.

Material	Space Group	a (Å)	b (Å)	c (Å)	α (°)	β (°)	γ (°)	χ^2
Fe_7S_8 /	C2/C	12.00185	6.88428	13.18790	90	119.419	90	0.611
Fe_3S_4	FD3M	9.96841	9.96841	9.96841	90	90	90	
ZnS	F43M	5.406310	5.406310	5.406310	90	90	90	2.667
TiS_2	P3M1	3.397	3.397	5.747	90	90	120	0.939

Determination of Optimum pH

The results for the pH study are shown in Figure 7. As can be seen in Figure 7A, for the binding of Pb(II) to the Fe_7S_8 nanomaterial increased with as pH increased. A binding of 5% was observed at pH 2 and a maximum binding of 67% was observed at a pH of 6. The binding of Cu(II) to the Fe_7S_8 nanomaterial constant at 100% binding as the pH of the reaction increased from pH 2 to pH 6. The binding on Pb(II) and Cu(II) to the ZnS, is shown in Figure 7B, and remained unaffected throughout each pH with a binding above 80%. On the other hand, the

binding for TiS_2, both ions were strongly pH dependent which can be seen in Figure 7C. Both Pb(II) and Cu(II) started at approximately 100% binding at a pH 2 and decreased as the pH increased. At a pH 6, the percent binding for Pb(II) and Cu(II) was approximately 60% and 8%, respectively. Due to these results, the optimum binding for both Fe_7S_8 and ZnS was determined to be a pH 5, while the optimal pH for the binding of Pb(II) and Cu(II) to TiS_2 was determined to be pH 2. A pH 6 was not chosen for the binding due to the possible formation of $Pb(OH)_2$ and $Cu(OH)_2$ at higher concentrations. These pH's were selected as the optimum binding and used for all further studies.

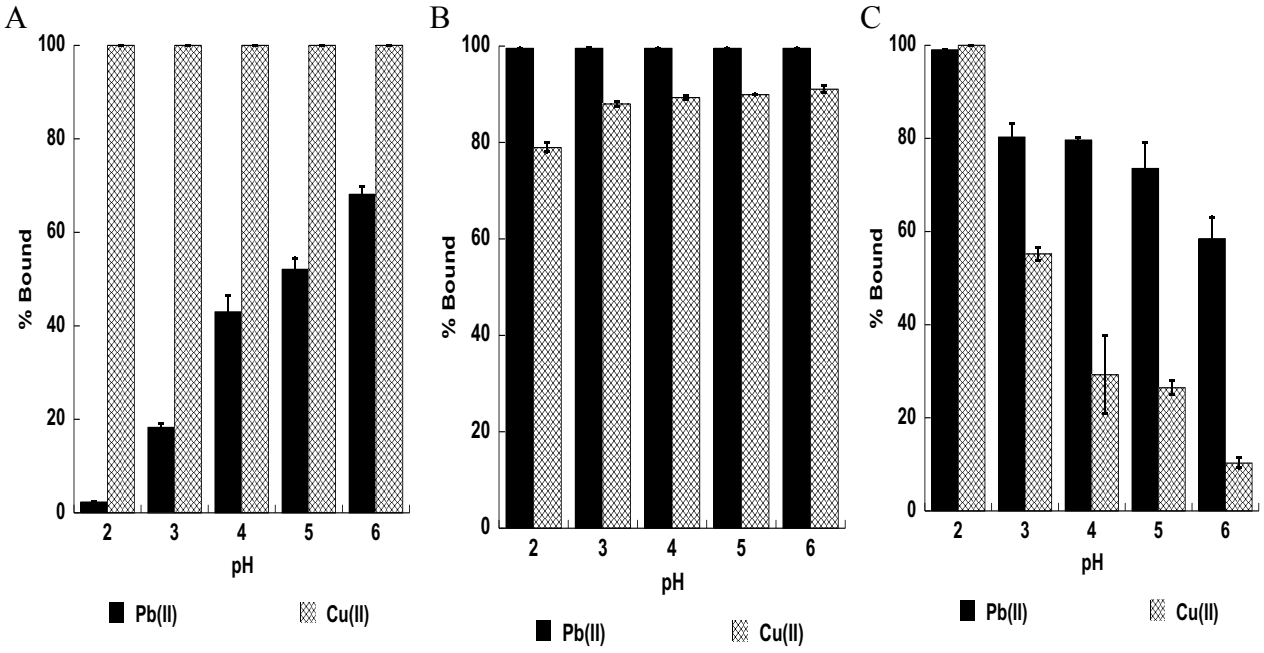

Figure 7: pH profile for the binding of Pb(II) and Cu(II) to the A) Fe_7S_8, B) ZnS (ambient light), C) TiS_2 nanomaterials.

Due to ZnS being photocatalyst, pH profile studies were performed under UV-light and in the absence of light to observed the possible effects on the metal binding. The results from the light and dark study are shown in Figure 8. The use of a Hg lamp producing UV-lighting showed no effect on the sorption of Pb(II) and Cu(II) as seen on Figure 8A. The sorption of Pb(II)

remained constant above an 80% binding throughout all pH's tested. A pH 6 for Pb(II) wasn't tested due to the precipitation of the lead as $Pb(OH)_2$. The binding of Cu(II) was approximately 80% at pH 2 and increased to 100% at pH 3 and remained constant thereafter. A similar effect occurred in the binding study performed in the dark shown in Figure 8B for the sorption of Cu(II). The Cu(II) binding was constant above 90% throughout all pH's tested. The sorption of Pb(II) on the other hand, began at 100% at pH 2 and decreased to approximately 50% binding thereafter. Due to these results, the UV-light studies and the sorption of Cu(II) in the absence of light and in the presence of UV-light were no longer an issue. The pH chosen for further studies on the sorption of Pb(II) was pH 5 due to the difference between the normal pH study and the "dark" pH study.

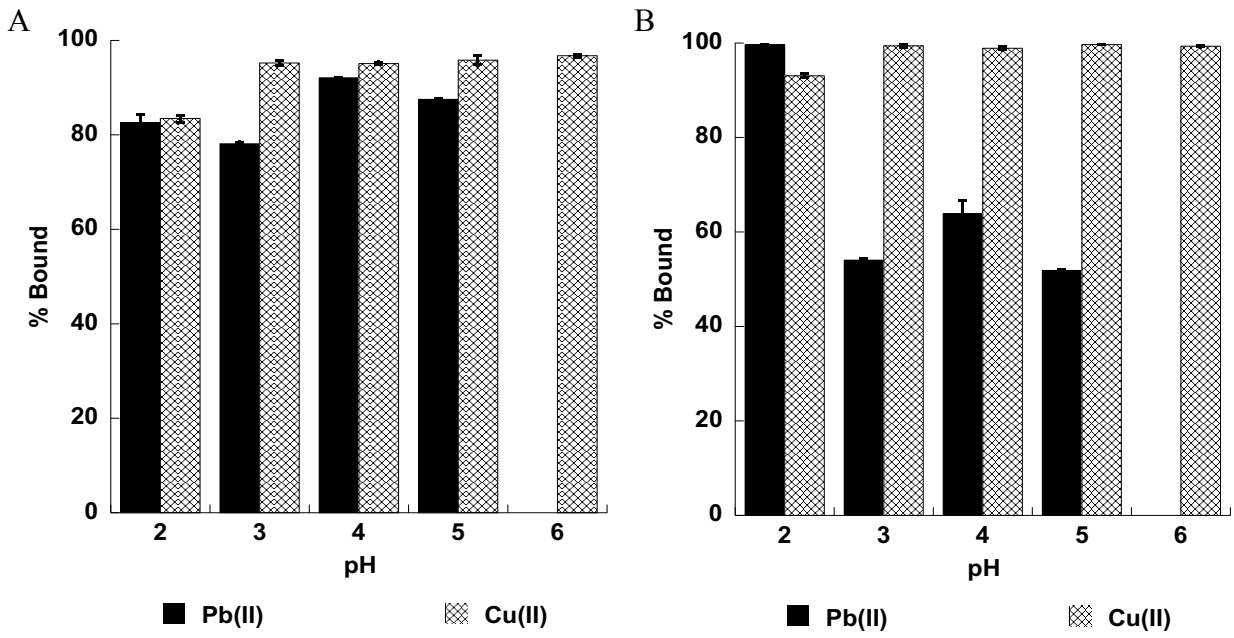

Figure 8: pH profile for the binding of Pb(II) and Cu(II) to the ZnS nanomaterial in the A) presence of UV-light, B) Absence of light (Dark).

The pH profile studies for the binding of Pb(II) and Cu(II) with Fe_7S_8 and ZnS in ambient light and ZnS in the presence of UV-light are in agreement with other results in literature

articles[10,14,15,26,27]. For instance, Tamez et al, showed that the binding of Pb(II) with Fe_3O_4 was pH independent above a pH 2 and the sorption of Cu(II) showed an increase in the binding as the pH increased[10]. Mahdavi et al, also showed a similar trend in the binding of Pb(II) and Cu(II) using Fe_3O_4, ZnO, and CuO. It was determined that the binding of Pb(II) and Cu(II) with Fe_3O_4 and CuO increased as the pH increased whereas for the binding to ZnO remained relatively pH independent[17]. The sorption of Pb(II) and Cu(II) to TiS_2 doesn't correlate to results discussed in literature.

Time Dependency Studies

The effect of time on the binding is an important factor in order to determine the minimum time required for the optimal removal of Pb(II) and Cu(II). The results of the time studies are shown in Figure 9. Figure 9A shows that the adsorption of both Pb(II) and Cu(II) to Fe_7S_8 increased as the time of equilibration increased. The binding of Pb(II) remained constant with 15% removed for the first 15 min of equilibration and steadily increased to a maximum of 40% removed after 240 min of equilibration. Cu(II) started with 5% removal at 5 min of contact time and increased to a maximum of 30% after 60 min of equilibration.

The binding of Pb(II) and Cu(II) to ZnS are shown in Figure 9B. The results show that the binding of Cu(II) was time independent and remained constant above 95% throughout all time intervals. Similarly, the binding of Pb(II) to ZnS in ambient light was determine to be time independent and after 5 min of contact time and a removal of 100% of the Pb(II) was observed. On the other hand, ZnS in the absence of light, showed different effects, and the results are shown in Figure 9C. For instance, in the absence of light, the binding of Pb(II) was determined to depend on time. The reaction started with approximately 35% removal within the first 5 min of contact and increased to 85% removal at a contact time of 60 min and beyond.

TiS_2 shared a similar trend to Fe_7S_8 where the binding of Pb(II) and Cu(II) were both observed to be time dependent. The results for the binding are shown in Figure 9D where binding of Pb(II) started off with approximately 5% binding at 5 min of contact and it remained relativelt constant up to 60 min of contact time. After 60 minutes of contact the binding increased to a maximum of 40% binding at 240 min of contact. Whereas, the sorption of Cu(II) began around 35% within the first 5 min of contact and was observed to increase with increasing contact time. The maximum binding occurred with 60 min of contact time and remained constant thereafter.

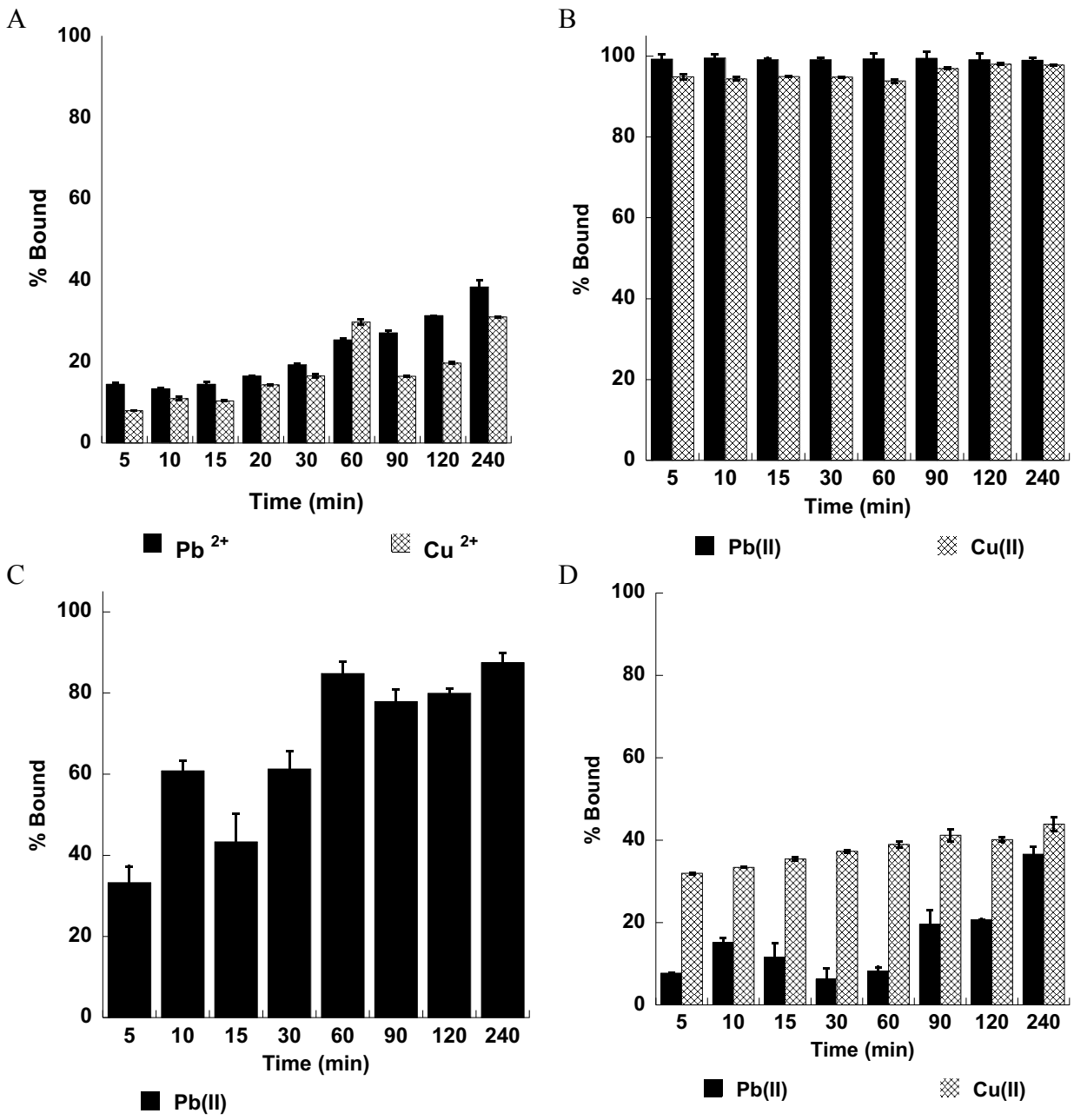

Figure 9: Time dependency of Pb(II) and Cu(II) binding to the A) Fe_7S_8 nanomaterial, B) ZnS nanomaterial in ambient light, C) ZnS nanomaterial dark conditions, D) TiS_2 nanomaterial.

The sorption of both Pb(II) and Cu(II) with Fe_7S_8, ZnS in absence of light, and TiS_2 are in agreement with trends observed in the literature various metal oxides and nano-adsorbents, the binding has been observed to increase with longer contact[15,17,28-31]. The sorption of both ions

onto ZnS in ambient light also corresponds to trends observed in the literature where the binding remains constant throughout the study[10,14,17].

Adsorption Kinetics

In order to determine the order and rate of the reaction, adsorption kinetic studies were conducted at two additional temperatures. The additional binding reactions were conducted at 4˚C and 45˚C. To determine the rate constant for the sorption process between Pb(II) and Cu(II) and each material—Fe_7S_8, ZnS, and TiS_2—the data was initially plotted using the percent remaining in solution after reaction against time. The data was observed to plot linear without any further manipulation. The equation for zeroth order kinetics is as follows:

$$[C] = k[t]$$

where c is the concentration at a given time, t is the time for adsorption in minutes, and k is the rate constant for the adsorption of the metal ion to the surface of the adsorbent at equilibrium. The reaction rates for each material are shown in Table 6 and 7 with the exception of ZnS in ambient lighting.

The sorption of both Pb(II) and Cu(II) with Fe_7S_8 was determined to follow zero order kinetics model, which the binding is directly dependent on the amount of contact time. The rates for the reactions increased as the temperature increased due to more molecular collisions occurring.

The sorption of Pb(II) and Cu(II) with ZnS in ambient light appeared to be unaffected with the amount of contact time, therefore no kinetics model could be developed. On the other hand, the adsorption of Pb(II) with ZnS in the absence of light was determined to follow a zeroth

order kinetics model. For this process, the rate of the reaction increased with an increase in temperature therefore and indicates an endothermic process for the reaction.

Similarly, the binding between Pb(II) or Cu(II) with TiS_2 also appeared to follow a zeroth order kinetics model with an increase in the reaction rates with higher temperatures. Such increase in reaction rates can be attributed to an increase in molecular collisions.

Table 3: Reaction rates for the sorption of Pb(II) with each transition metal sulfide nanomaterial.

Metal Sulfide	T (K)	Equation	R^2	Ea(kJ/mol
Fe_7S_8	277	0.0832x+13.49	0.986	23.6
	296	0.1533x+14.04	0.980	
	318	0.3033x+31.52	0.989	
ZnS (Dark)	277	0.2232x+33.98	0.992	19.4
	298	0.3531x+47.48	0.987	
	316	0.6609x+63.95	0.982	
TiS_2	277	0.809x+77.04	0.990	54.1
	296	1.667x+5.12	0.970	
	318	17.422x-72.4	0.991	

Table 4: Reaction rates for the sorption of Cu(II) with each transition metal sulfide nanomaterial.

Metal Sulfide	T (K)	Equation	R^2	Ea(kJ/mol
Fe_7S_8	277	0.063x+5.39	0.986	45.1
	296	0.1276x+9.49	0.980	
	318	0.7604x+51.59	0.989	
ZnS	N/A	N/A	N/A	N/A
TiS_2	277	0.971x+135.7	0.990	19.7
	296	1.433x+392.0	0.990	
	318	2.947x+415.4	0.989	

The Arrhenius plots for the reactions between the Pb(II) and Cu(II) with the metal sulfides are shown in Figures 10-11. Since the sorption of Pb(II) and Cu(II) with ZnS in ambient did not have a kinetics model and due to complete binding within 5 min of contact time and remained constant thereafter, an Arrhenius plot could not be constructed. The correlation

coefficients for each plot are 0.98 or better. The Arrhenius plots were then used to determine the activation energies for the binding of Pb(II) and Cu(II) onto each transition metal sulfide nanomaterial. The activation energies are presented in the kinetics tables, Table 6 and 7 for Pb(II) and Cu(II) ions, respectively. The activation energies for the sorption of Pb(II) and Cu(II) with Fe_7S_8 were calculated to be 23.6 kJ/mol and 45.1 kJ/mol, respectively. The activation energy for the sorption of Pb(II) with ZnS in the absence of light exhibited a similar binding energy of 20.53 kJ/mol. On the other hand, the binding of Pb(II) with TiS_2 showed a slightly higher activation energy of 54.1 kJ/mol. The binding of Cu(II) with TiS_2 however was lower than Fe_7S_8 with an energy of 19.77 kJ/mol.

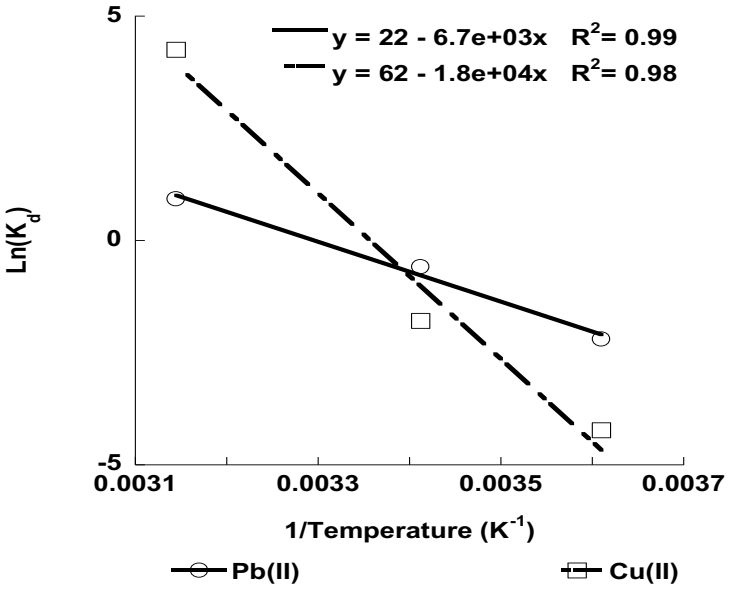

Figure 10: Arrhenius plot for the sorption of Pb(II) and Cu(II) onto the Fe_7S_8 nanomaterial.

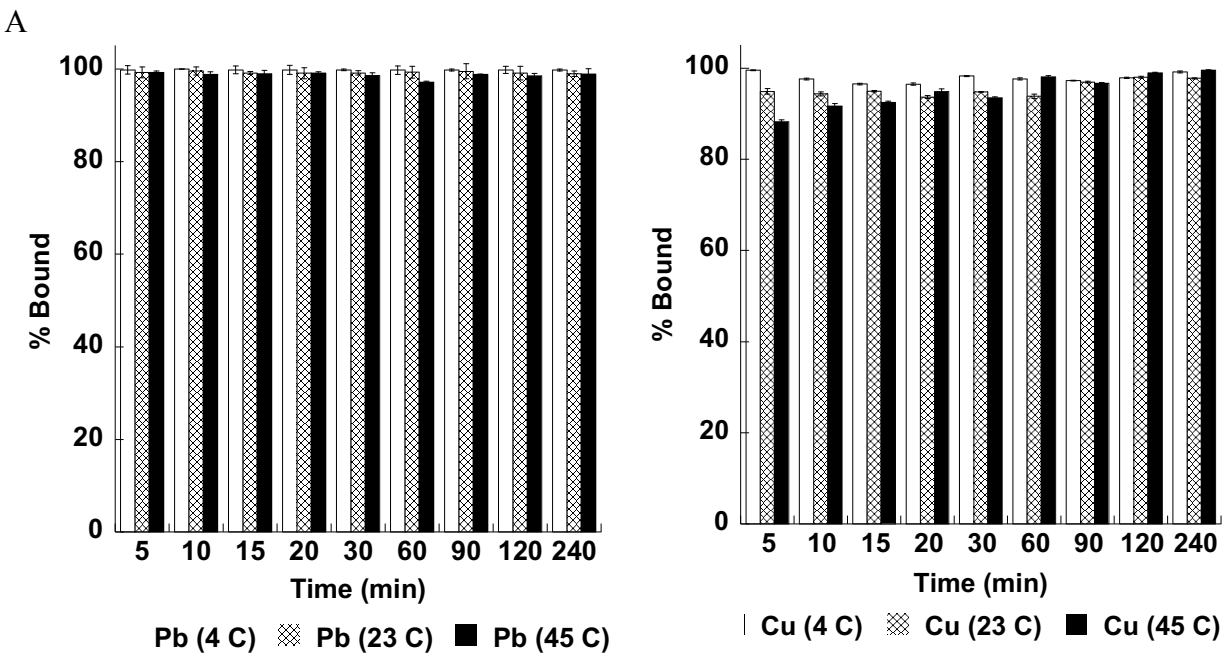

Figure 11: Time dependence at various temperatures for the binding of A) Pb(II) and B) Cu(II) with ZnS in the presence of ambient light.

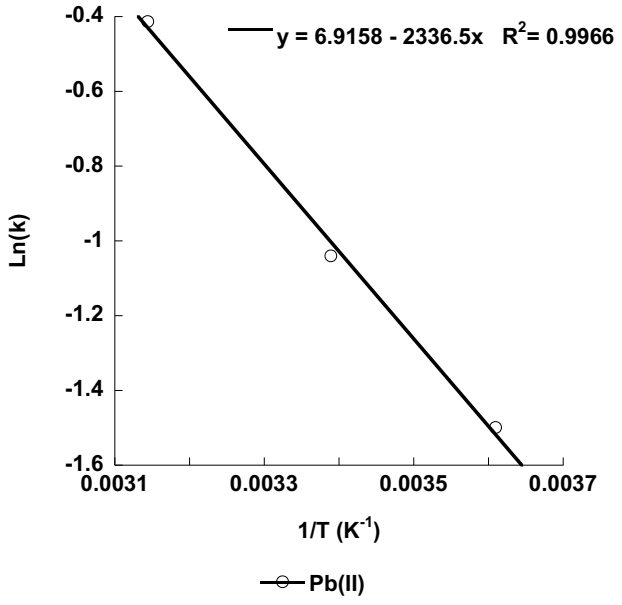

Figure 12: Arrhenius plot for the sorption of Pb(II) onto the ZnS nanomaterial in the absence of light.

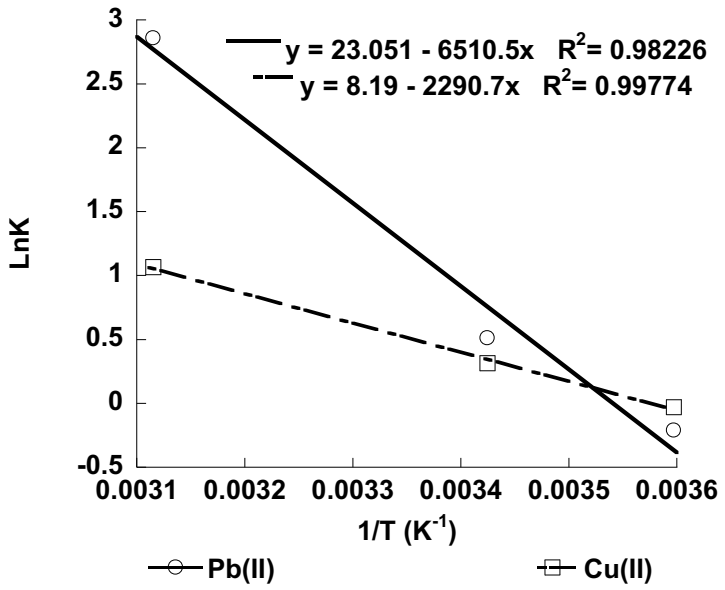

Figure 13: Arrhenius plot for the sorption of Pb(II) and Cu(II) onto the TiS_2 nanomaterial.

Adsorption Capacities Study

The maximum capacity for removal of each material was determined using the Langmuir isotherm model. The capacity was calculated using the linearized Langmuir isotherm model which is shown below:

$$\frac{1}{q_e} = \frac{1}{q_m} + \frac{1}{K_a q_m C_e}$$

where q_e is the removal capacity at a given concentration, q_m is the maximum binding capacity, K_a is constant, C_e is the equilibrium concentration of the solution after binding. The capacity studies were conducted at three temperatures 4˚C, 21˚C, and 45˚C. The capacities for each material are shown in Tables 3-5. For the most part, the Pb(II) and Cu(II) binding to the materials appeared to follow the same trend in which the maximum capacity for both ions

increased as the temperature increased. However, the binding of Cu(II) to the TiS_2 nanomaterial showed a reverse binding trend, a decrease with increasing temperature. ZnS had the highest binding capacity of the three materials tested for lead binding at room under light conditions. The decrease observed in the binding of Pb(II) under the dark conditions compared to the binding in the presence of light could be attributed to the photo-properties of the ZnS and the photo-properties of lead sulfide. PbS is a possible product for the reaction between Pb(II) with transition metal sulfide nanoparticles. However, it should be noted that the results of the binding study indicate the binding of Pb(II) to the transition metal sulfide nanoparticles is an endothermic process.

The binding of Cu(II) ions to the Fe_7S_8 and ZnS followed the same trend as the Pb(II) ions. The binding of the Cu(II) ions to the Fe_7S_8 and ZnS nanomaterials showed an increase in the binding with increasing temperature, again indicating an endothermic reaction was occurring. However, the binding of the Cu(II) ions to the TiS_2 showed the opposite trend a decrease in the binding was observe with the increase in reaction temperature. The binding of Cu(II) ions decreased from approximately 250 mg/g at 4˚C to approximately 161 mg/g at 45˚C. The decrease in binding with increasing temperature indicates the Cu(II) binding reaction is exothermic in nature. The decrease in binding may be due to the low pH used for the binding, a pH of 2, increases in acidity have been shown to affect the formation of particular transition metal sulfides, and in fact increasing the solubility of the metal sulfide. Unlike Pb(II) which forms one sulfide for PbS, Cu forms many different polysulfide materials when reacted with sulfur. The observed decrease in the Cu(II) ion binding may be a side effect of multiple reactions occurring, which increase the solubility of the Cu(II) with increasing temperature.

Comparing the binding data for both metals, in mmol/g shows that over all the Cu(II) ion is preferentially bound to all the nano-metal sulfides. With all the materials at all temperatures, Cu(II) shows a much higher binding capacity in mmol/g than the Pb(II) ions. This may also be a function of the different types of Cu(II) sulfides that can form compared with Pb(II).

Table 5: Binding capacity of the Fe_7S_8 nanomaterial for the Pb(II) and Cu(II) using the Langmuir Isotherm model.

Material	Ion	Temperature (K)	Capacity (mg/g)	Capacity (mmol/g)
Fe_7S_8	Pb(II)	277 K	6.23	0.030
		295 K	8.09	0.039
		318 K	21.4	0.103
	Cu(II)	277 K	1.31	0.073
		295 K	5.29	0.102
		318 K	116.3	1.92

Table 6: Binding capacity of the ZnS nanomaterial for the Pb(II) and Cu(II) using the Langmuir Isotherm model.

Material	Ion	Temperature (K)	Capacity (mg/g)	Capacity (mmol/g)
ZnS (ambient light)	Pb(II)	277 K	39.1	0.189
		295 K	128.2	0.619
		318 K	147.1	0.710
	Cu(II)	277 K	116.3	1.83
		295 K	212.8	3.35
		318 K	243.9	3.84
ZnS (Dark)	Pb(II)	277 K	36.1	0.174
		295 K	54.1	0.261
		318 K	79.4	0.383

Table 7: Binding capacity of the TiS_2 nanomaterial for the Pb(II) and Cu(II) using the Langmuir Isotherm model.

Material	Ion	Temperature (K)	Capacity (mg/g)	Capacity (mmol/g)
TiS_2	Pb(II)	277 K	27.7	0.13
		295 K	107.5	0.52
		318 K	333.3	1.61
	Cu(II)	277 K	250.0	3.93
		295 K	217.0	3.42
		318 K	161.3	2.54

The results for the sorption of Pb(II) and Cu(II) with other transition metal oxides and nano-adsorbents have shown variable data[8,14-15, 32]. For example, CuO nanomaterial for the binding of Pb(II) and Cu(II) has exhibited capacities of 39.4 mg/g and 54.1 mg/g, respectively[17]. Additionally, CeO_2 has proven to have low binding capacities of 9.2 mg/g and 15.4 mg/g for both Pb(II) and Cu(II)[33]. Similarly, Fe-water treatment residues were showed to have capacities in the same range as CeO_2 where the capacity for Pb(II) was 22 mg/g and Cu(II) was 6 mg/g[32]. Nadaroglu et al., proved that the sorption of Cu(II) onto red mud showed a similar capacity as Fe_7S_8 with a capacity of 5.35 mg/g[34]. On the other hand, graphene oxide has been proven to have high binding capacities of 294, 530, 345, and 1119 mg/g for Cu(II), Cd(II), Zn(II), and Pb(II) respectively[15].

Thermodynamics Study

The thermodynamic parameters for each adsorption process was determined from isotherm studies performed at temperatures of 4˚C, 22˚C, and 45˚C the same experiments used to determine the binding capacities. All sorption processes were found to follow the Langmuir isotherm model as previously mentioned. Figures 14-17 show the thermodynamic plots developed from the isotherm data collected at 4˚C, 22˚C, and 45˚C. The plots, of the thermodynamics of the reaction were determined using the following equations:

$$\Delta G = \Delta H - T\Delta S$$

Where ΔG is the Gibbs free energy of the process, ΔH is the enthalpy of the binding process, T is the temperature of the process in Kelvin (K), and ΔS is the entropy of the process. However, ΔG can be related to the equilibrium constant through the following equation

$$\Delta G = -RTLn(K_d)$$

Where ΔG is the Gibbs free energy of the process, R is the Gas constant (8.314 J K-1mol-1), T is the temperature in Kelvin (K), and LnK_d is the natural log of the distribution coefficient.

Through substitution of $-RTLn(K_d)$ into equation containing enthalpy and entropy the following equation is developed, which relates the distribution constant to the entropy and enthalpy

$$Ln(K_d) = \frac{\Delta S}{R} - \frac{\Delta H}{RT}$$

where the ΔG is the Gibbs free energy; R is the gas constant (8.314 J K^{-1} mol^{-1}); T is the absolute temperature in Kelvin; K_d is the distribution coefficients; ΔS is the change in entropy; ΔH is the change in enthalpy.

The ΔG for the process can be calculated directly from the distribution coefficient, which is equal to the inverse of the slope obtained from the isotherm plots. Whereas, ΔH and ΔS were determined by plotting the LnK_d against 1/T (in K). Where the slope of the line and intercept of the plot represent the ΔH and ΔS of the process, respectively. Furthermore, the calculated thermodynamic parameters for the binding reaction are shown in Tables 8-10.

The sorption process for Pb(II) and Cu(II) with the Fe_7S_8 nanomaterial is shown in Table 6 and it shows the ΔG, ΔH, and ΔS for each ion. For the binding of Pb(II) the ΔG decreases from 5.07 kJ/mol to -2.45 kJ/mol from 4˚C to 45˚C showing that the process is spontaneous higher

temperatures and non-spontaneous at lower temperatures. The decrease in the ΔG with increasing temperatures indicates that the process is endothermic in nature. A similar trend was observed with the ΔG of binding for the Cu(II) with Fe_7S_8 decreased from 9.87 kJ/mol to -11.23 from 4˚C to 45˚C showing that the sorption process again more favorable at higher temperatures indicating an endothermic reaction. The ΔH for the binding of Pb(II) was 55.81 kJ/mol and it showed that the sorption was endothermic for Pb(II). Similarly, the ΔH for the binding of Cu(II) was at 153.51 kJ/mol also describing an endothermic process. Furthermore, the magnitude of the enthalpy describes the type of process for the sorption in which energy values below 40 kJ/mol correspond to physisorption processes, energy values above 40 kJ/mol are attributed to chemisorption processes, and chemical ion exchange processes correspond to energies from 8.0 to 16 kJ/mol. Based on the magnitude of ΔH, the sorption process for Pb(II) and Cu(II) occurred through chemisorption[35]. Additionally, the ΔS for the binding of Pb(II) and Cu(II) onto Fe_7S_8 was 83.61 J/mol and 515.5 J/mol. The positive entropy indicates an increase in the entropy of the systems entropy which may be attributed to the release of water molecules or other species bound on the surface of the nanomaterial and the formation of the final product.

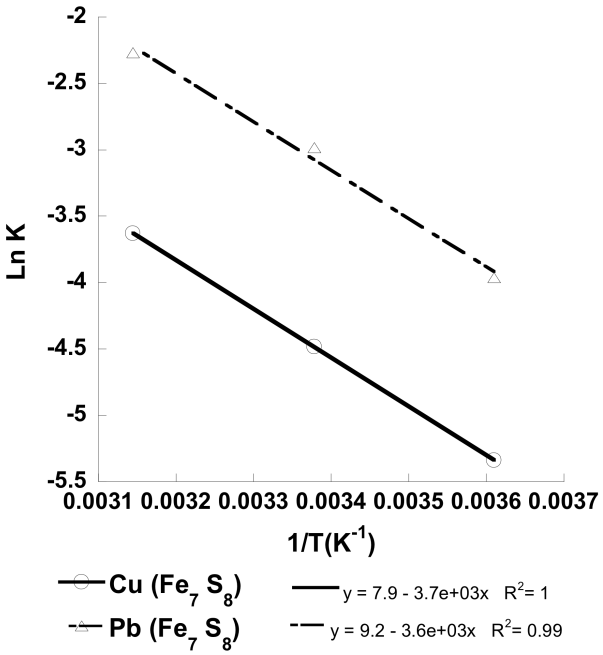

Figure 14: Isotherm plot for the binding of Pb(II) and Cu(II) to the Fe_7S_8 nanomaterial.

Table 8: Thermodynamic parameters for the binding of Pb(II) and Cu(II) to the Fe_7S_8 nanomaterial.

Ion	**ΔG (kJ/mol)**	**ΔH (kJ/mol)**	**ΔS (J/mol)**
Pb(II)	5.01 (277 K) 1.44 (295 K) -2.45 (318 K)	55.81	183.6
Cu(II)	9.87 (277 K) 4.60 (295 K) -11.23 (318 K)	153.5	515.5

The thermodynamic parameters for the binding of Pb(II) and Cu(II) to the ZnS nanomaterial in different conditions are shown in Table 7. The ΔG for the binding of Pb(II) in ambient light increases decreased from -4.93 kJ/mol to -9.98 kJ/mol from 4˚C to 45˚C indicating that the sorption process spontaneous and endothermic. Similarly, the ΔG for the binding of Cu(II) in ambient light decreased from -6.93 kJ/mol to -13.12 kJ/mol showing a spontaneous process increasing with increasing temperature. The calculated ΔH values for the adsorption of

Pb(II) and Cu(II) onto ZnS in ambient lighting were 30.86 kJ/mol and 38.89 kJ/mol indicating an endothermic process for the binding both Pb(II) and Cu(II). These energy values may indicate the sorption process for Pb(II) and Cu(II) ions is through physisorption[32]. The change in entropy for the removal of Pb(II) and Cu(II) with ZnS in ambient lighting was 128.87 J/mol and 162.95 J/mol. The positive entropy could be attributed to the release of protons or other species into solution upon the removal of Pb(II) and Cu(II). In the absence of light for the binding of Pb(II) a similar trend was observed a decreasing the ΔG with increasing temperature, from -2.81 kJ/mol to -5.56 kJ/mol from 4˚C to 45˚C indicating a endothermic process. The ΔH of the binding process was 16.21 indicating the binding was endothermic and occurring thorough ion-exchange process and physisorption[32]. There was also a positive change in the ΔS again indicating that there is a release of protons or other species into solution upon the removal of Pb(II)

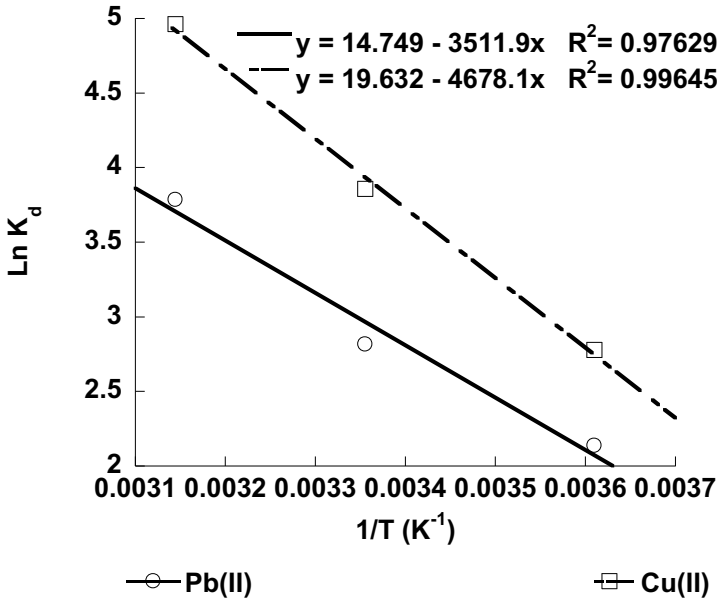

Figure 15: Isotherm plot for the binding of Pb(II) and Cu(II) to the ZnS nanomaterial in ambient lighting.

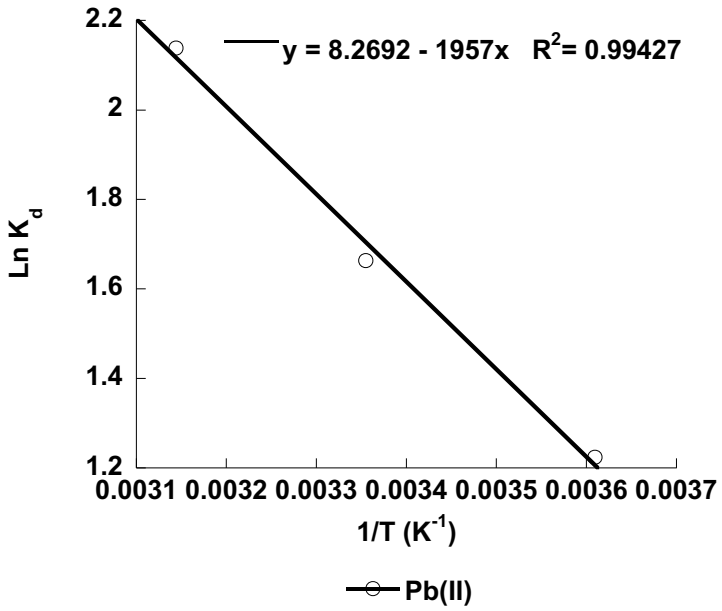

Figure 16: Isotherm plot for the binding of Pb(II) to the ZnS in the absence of lighting.

Table 9: Thermodynamic Parameters for the binding of Pb(II) and Cu(II) to the ZnS nanomaterial.

Material	**Ion**	**ΔG (kJ/mol)**	**ΔH (kJ/mol)**	**ΔS (J/mol)**
ZnS (Ambient light)	Pb(II)	-4.93 (277 K) -6.84 (298 K) -9.98 (315 K)	30.86	128.87
	Cu(II)	-6.39 (277 K) -9.55 (298 K) -13.12 (318 K)	38.89	162.95
ZnS (Dark)	Pb(II)	-2.81 -4.06 -5.56	16.21	68.75

The calculated thermodynamic parameters for the binding of Pb(II) and Cu(II) onto TiS_2 are shown in Table 8. The ΔG values for the binding of Pb(II) ranged from -2.55 to -16.33 kJ/mol from 4˚C to 45˚C, respectively. The ΔG values indicate a spontaneous endothermic reaction occurs for the binding of Pb(II). However, the ΔG values for the sorption of Cu(II) increased from -0.003 to 2.0 kJ/mol for 4˚C to 45˚C, respectively. These values indicated that the sorption process was close to equilibrium however the binding process was exothermic in nature. Furthermore, the ΔH for the sorption of both Pb(II) and Cu(II) were calculated to be 95.8 kJ/mol and -14.24 kJ/mol, respectively. The positive ΔH indicates for Pb(II) binding indicates an endothermic process occurring. However, the negative ΔH values for Cu(II) indicates an exothermic process. The magnitude of the ΔH may be indicating that the sorption of Pb(II) occurs though chemisorption while the sorption process for Cu(II) is occurring through ion-excahnge[35]. The values for the entropy for the binding of Pb(II) and Cu(II) to TiS_2 were 355.8 J/mol and -51.4 J/mol, respectively. The increase in entropy for Pb binding may be corresponding to the release of protons upon removal of such heavy metal ions. However, the negative ΔS for the copper binding may be explained though less ions are in solution after Cu(II) binding, Cu(II) reacting with S is known to have multiple species and products that may react and bind other species in solution resulting in less entropy of the system.

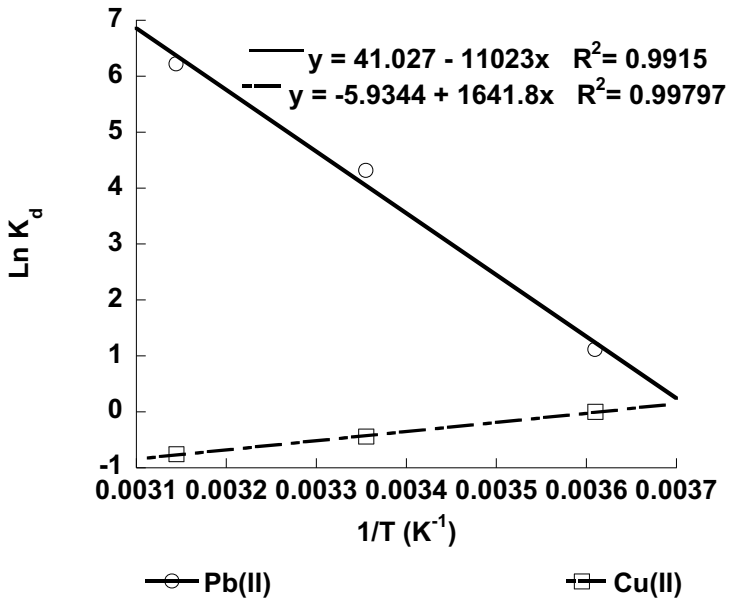

Figure 17: Isotherm plot for the binding of Pb(II) and Cu(II) onto TiS_2 nanomaterial.

Table 10: Thermodynamic parameters for the binding of Pb(II) and Cu(II) to the TiS_2 nanomaterial.

Ion	**ΔG (kJ/mol)**	**ΔH (kJ/mol)**	**ΔS (J/mol)**
Pb^{2+}	-2.55 (277 K) -10.68 (298 K) -16.33 (318 K)	95.8	355.8
Cu^{2+}	-0.003 (277 K) 1.10 (298 K) 2.00 (318 K)	-14.24	-54.1

In past studies, the sorption processes have been mostly spontaneous and endothermic similar to the results from the current study; with the exception of Cu(II) binding to the TiS_2 nanomaterial. For instance, the sorption of Cu(II) and Pb(II) onto manganese oxide coated sand showed ΔG values ranging from -16.0 kJ/mol to -19.4 kJ/mol for temperature ranges of 288K to 318 K and -16.2 kJ/mol to -18.9 kJ/mol for temperatures between 295 K to 318 K indicating that the sorption process was spontaneous[36]. Similarly, the binding of Pb(II) and Cu(II) with meranti wood sawdust showed a decrease in ΔG with an increase in temperature from -20.99 kJ/mol to -

25.16 kJ/mol and -21.09 kJ/mol to -26.40 kJ/mol respectively[12]. In addition, the binding of Cu(II) with pomegranate peel was determined to be spontaneous at high temperatures with ΔG values of -5.358 kJ/mol and -7.409 kJ/mol at temperatures of 303 K and 313 K, respectively[37].

Binding Interference Studies

Since all natural water systems contain minerals and ions present, the effects of the common cations present in real world water systems were tested for their effect on the Pb(II) and Cu(II) binding. Figure 18 shows the effects of Na^+, K^+, Ca^{2+}, or Mg^{2+} ions present on the sorption of Pb(II) and C(II) with Fe_7S_8. Based on the results shown in Figure 18A, the presence of Na^+ in the sorption process for Pb(II) showed little to no effect on the binding with a constant binding of 40% with increasing concentration from 0.3 ppm to 100 ppm. However, at higher concentrations above 100 ppm a synergistic effect occurred in which the binding of Pb(II) increased to 50%. In the presence of the other cations: K^+, Ca^{2+}, and Mg^{2+}, the binding of Pb(II) little to no effect was observed as the interfering ions concentrations were increased. For instance, the binding of Pb(II) in the presence of 0.3 ppm K^+ started with approximately 30% binding and remained constant as the concentration of K^+ increased to 1000 ppm. Similarly, the binding of Pb(II) with Ca^{2+} or Mg^{2+} present, started around 40% binding and did not change throughout the study. However, as can be seen in Figure 18B, the presence of Na^+, Ca^{2+}, and Mg^{2+} with increasing concentration showed an antagonistic effect on the binding on Cu(II). Cu(II) binding in the presence of 0.3 ppm Na^+, the binding was approximately 97% and the increase in Na^+ caused a decrease in binding by 10% leading to a binding of 87% with 1000 ppm Na^+. Similarly, the increase in concentration of Ca^{2+} or Mg^{2+} cause a decrease in binding by 30%

and 40%, respectively from 3 ppm to 1000 ppm. On the other hand, the presence of K^+ with increasing concentration had little to no effect on the binding of Cu(II) onto Fe_7S_8.

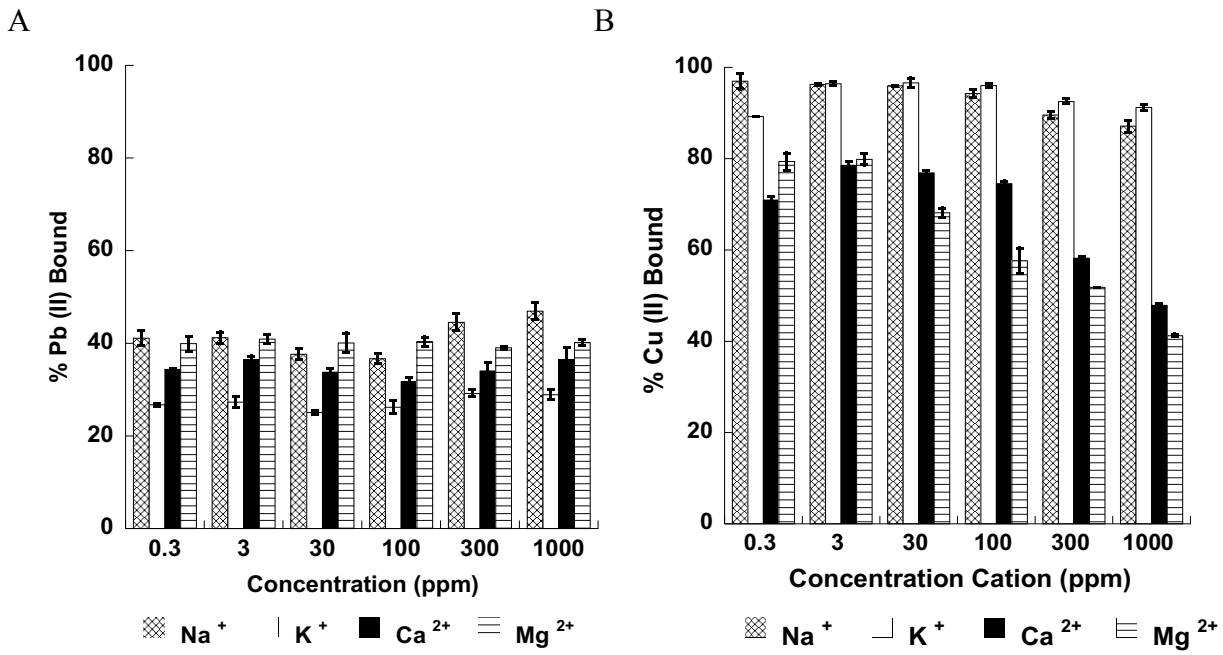

Figure 18: Effects on interference ions onto the binding of Pb(II) and Cu(II) with the Fe_7S_8 nanomaterial.

Figure 19 shows the effects of Na^+, K^+, Ca^{2+}, or Mg^{2+} ions present on the sorption of Pb(II) and Cu(II) onto ZnS in ambient light. The presence of Na^+, K^+, Ca^{2+}, or Mg^{2+} showed no effect with increasing concentration on the binding of Pb(II). The sorption of Pb(II) in the presence of any of the cations remained constant with approximately 90% binding. The sorption of Cu(II) in the presence of Na^+ and K^+ remained constant between 0.3 ppm and 100 ppm with 100% binding, in Figure 19B. At higher concentrations, the presence of such ions had an antagonistic effect and the binding of Cu(II) decreased to 85% and 94% at 1000 ppm of Na^+ and K^+, respectively. The presence of Ca^{2+} and Mg^{2+} also had an antagonistic effect on the sorption of Cu(II). In the presence of Ca^{2+}, the binding of Cu(II) was 81% at 0.3 ppm, the binding

increased to 89% in the presence of 3 ppm of Ca^{2+}. Above 3.0 ppm Ca^{2+}, the binding decreased steadily and resulted in 49% binding at 1000 ppm of Ca^{2+}. Similarly, the sorption of Cu(II) in the presence of 0.3 ppm Mg^{2+} was at 77% binding, however the binding increased to 83% in the presence of 3 ppm Mg^{2+}. As the concentration of Mg^{2+} continued increasing, the binding decreased gradually resulting in 44% Cu(II) binding in the presence of 1000 ppm Mg^{2+}. Furthermore, the effects of Na^{+}, K^{+}, Mg^{2+} or Ca^{2+} on the sorption of Pb(II) with ZnS (dark) are shown in Figure 20. The results for the interference study for ZnS in the absence of light were the same as the results given by the ambient light "regular" interference study with ZnS. The presence of any of the cations showed no effect on the binding as the concentration of the interfering ion increased in which the binding remained above 90%.

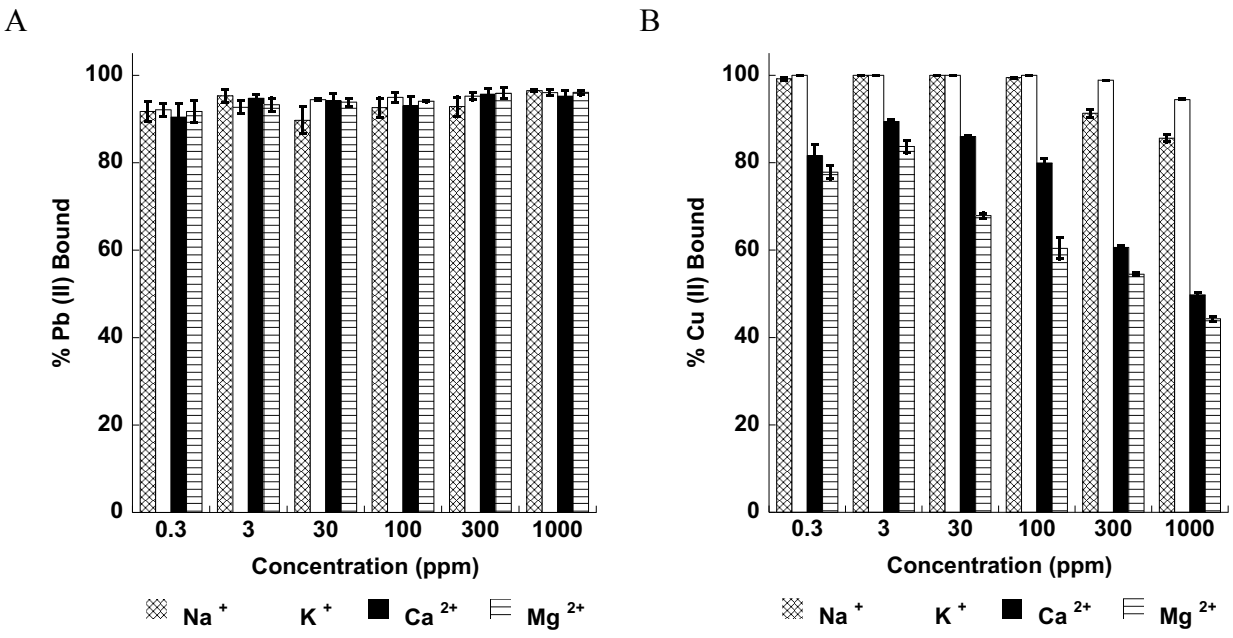

Figure 19: Effects on interference ions onto the binding of Pb(II) and Cu(II) with the ZnS nanomaterial in ambient lighting.

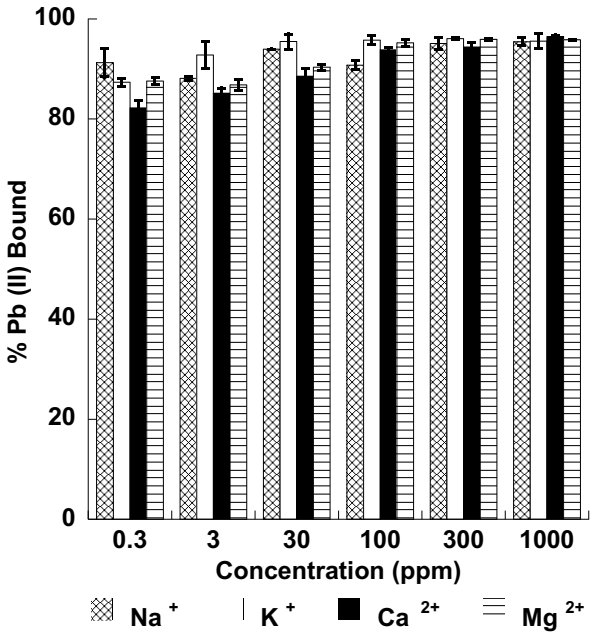

Figure 20: Effects on interference ions onto the binding of Pb(II) with the ZnS nanomaterial in the absence of light.

Figure 21 shows the effects of having Na^+, K^+, Ca^{2+}, or Mg^{2+} ions present in the sorption of Pb(II) and Cu(II) onto the TiS_2 nanomaterial. The presence of Na^+, K^+, and Ca^{2+} showed little to no effect on the sorption of Pb(II) as the concentrations were increased. The binding of Pb(II) in the presence of Na^+, K^+, and Ca^{2+} ions remained constant at 100% binding throughout all concentrations. The presence of Mg^{2+} showed no effect on the sorption from 0.3 ppm to 300 ppm and the binding 100%. However, at a Mg^{2+} concentration of 1000 ppm, the binding of Pb(II) decreased to approximately 95%. The sorption of Cu(II) shown in Figure 21B, was unaffected by the presence of 0.3 ppm to 100 ppm of Na^+, K^+, and Ca^{2+} in which the binding remained at 100%. At higher concentrations, the binding decreased to approximately 50%. In the presence of 0.3 ppm and 3 ppm Mg^{2+}, the sorption of Cu(II) started at approximately 80%. At 30 ppm Mg^{2+} a synergistic effect occurred and caused the binding to increase to 100%, but at 1000 ppm Mg^{2+} the binding decreased to 40%.

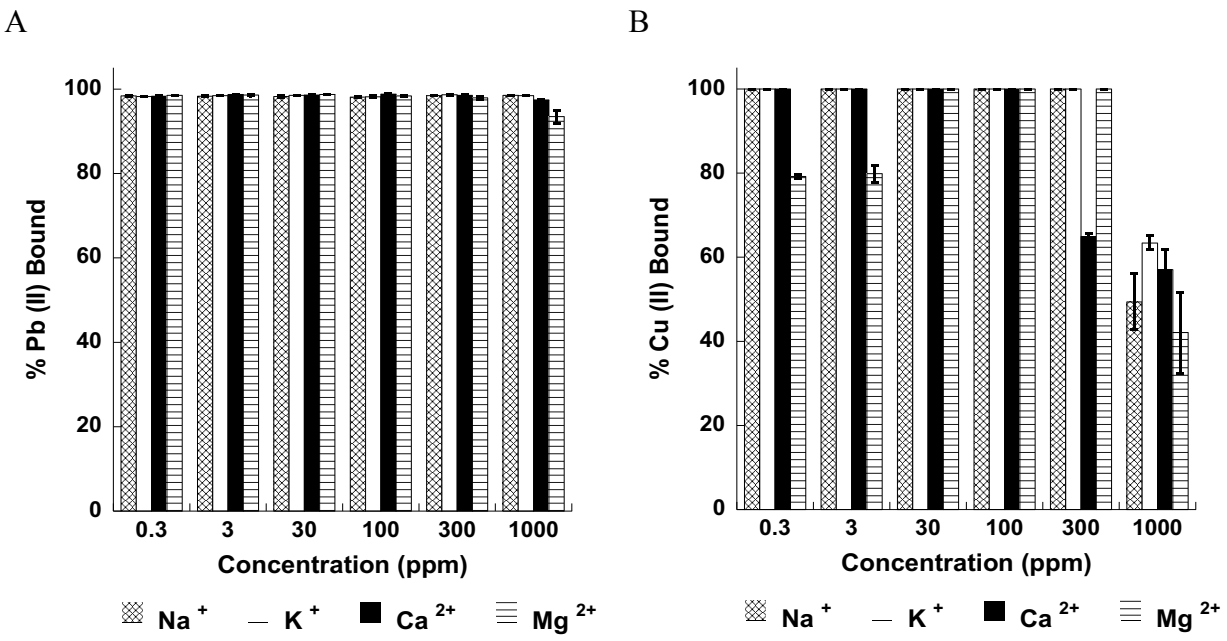

Figure 21: Effects on interference ions onto the binding of Pb(II) and Cu(II) with the TiS_2 nanomaterial.

A combination of all of the hard cations were investigated for their interference on the binding of Pb(II) and Cu(II) ions by the transition metal sulfides. Figure 22 shows the effects of increasing concentration of a combination of Na^+, K^+, Ca^{2+}, and Mg^{2+} onto the binding of Pb(II) and Cu(II) with Fe_7S_8. From the results, it can be observed that the binding of Pb(II) in the presence of 0.3 ppm was around 38% and it remained constant at approximately the same percent binding with increasing concentrations. On the other hand, the binding of Cu(II) in the presence of 0.3 ppm of all cations started at 60% and increased to approximately 70% at the 3 ppm concentration combination. Thereafter, the binding decreased steadily as the concentration of all cations increased. At 1000 ppm combination of cations, resulted in 32% binding of Cu(II).

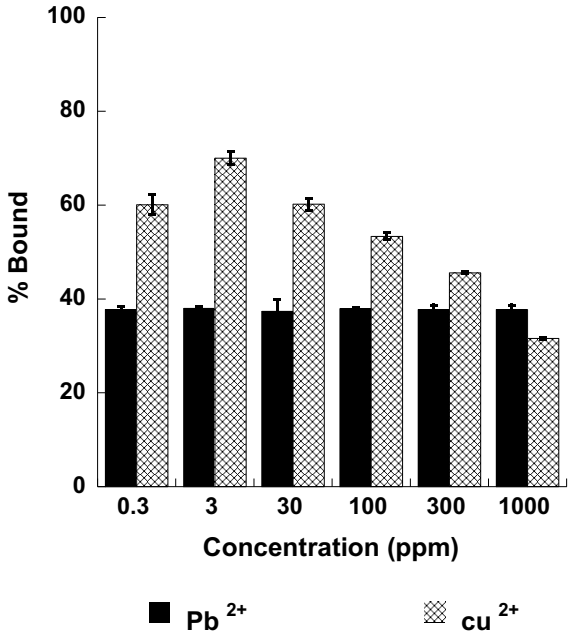

Figure 22: Effects of a combination of Na^{+}, K^{+}, Ca^{2+}, and Mg^{2+} with increasing concentrations on the binding of Pb(II) and Cu(II) with Fe_7S_8 nanomaterial.

The effects of a combination of cations at increasing concentrations on the sorption of Pb(II) and Cu(II) with ZnS in ambient light are shown in Figure 23. In the presence of 0.3 ppm of all cations, the binding of Pb(II) was approximately 88%. With an increase in concentration of the cations, the binding of Pb(II) showed a synergistic effect where the binding increased by 10% in the presence of the 1000 ppm combination. On the other hand, the sorption of Cu(II) with 0.3 ppm of all cations was approximately 98% and decreased as the concentration of the cations was increased. For example, the binding of Cu(II) with 30 ppm of the cations was around 64% and in the 1000 ppm combination, the binding decreased to 33%. Furthermore, the results for the presence of all cations on the sorption of Pb(II) with ZnS in "dark" conditions, shown in Figure 24, were similar to the results obtained by the ambient light conditions. The binding of Pb(II) with 0.3 ppm of all cations was 86% and the binding increased as the concentration of cations increased leading to a total of 97% binding with 1000 ppm interfering ions.

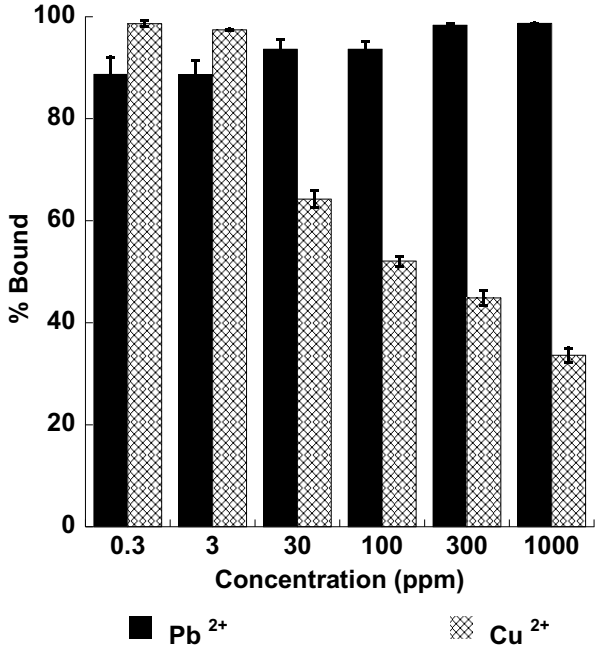

Figure 23: Effects of a combination of Na^{+}, K^{+}, Ca^{2+}, and Mg^{2+} with increasing concentrations on the binding of Pb(II) and Cu(II) with ZnS nanomaterial in ambient lighting.

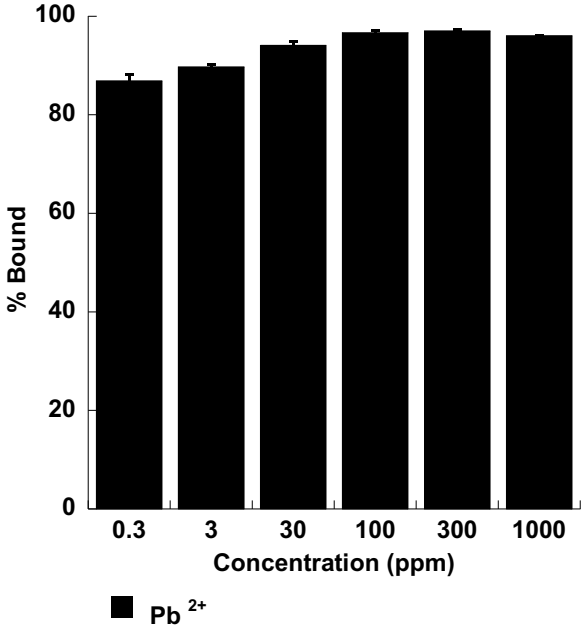

Figure 24: Effects of a combination of Na^{+}, K^{+}, Ca^{2+}, and Mg^{2+} with increasing concentrations on the binding of Pb(II) with ZnS (dark conditions) nanomaterial.

Figure 25 shows the sorption of Pb(II) and Cu(II) with TiS_2 with the combination of all four cations with increasing concentrations. The sorption of Pb(II) remained unaffected showing approximately 100% binding in the presence of all cations at all concentrations. Cu(II) on the other hand, started at 34% with 0.3 ppm combination and it remained rather constant with increasing concentrations. However, at 3 ppm and 300 ppm concentrations of the combination of all cations the binding increased to 63% and 52%, respectively.

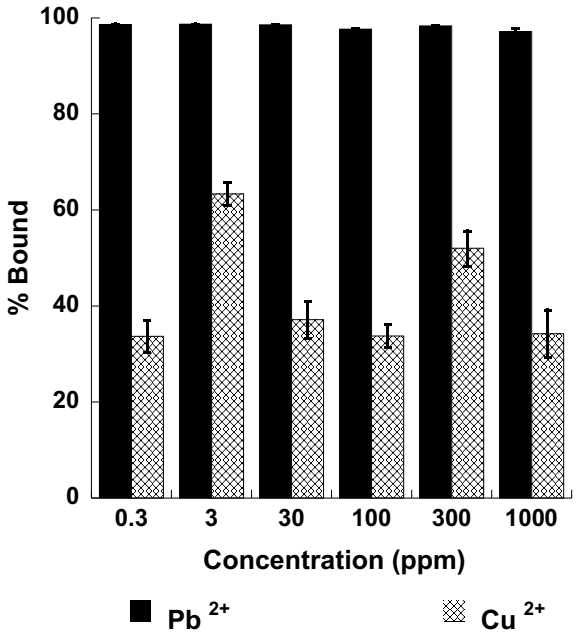

Figure 25: Effects of a combination of Na^+, K^+, Ca^{2+}, and Mg^{2+} with increasing concentrations on the binding of Pb(II) and Cu(II) with TiS_2 nanomaterial.

A study conducted by Tamez et al., showed that the sorption of Pb(II) onto Fe_3O_4 exhibited no interference in the presence individual solution and combinations of Na^+, K^+, Ca^{2+}, and Mg^{2+}. However, for the sorption of Pb(II) onto Fe_2O_3 the presence of Na^+ or Ca^{2+} created a synergistic effect in which the binding of Pb(II) increased as the concentration of either cation increased[10]. In the same study the binding of Cu(II) with Fe_3O_4, showed no effect in the presence

of any of the cations. However, the sorption of Cu(II) with Fe_2O_3 was affected negatively as the concentration of Mg^{2+} was increased. The presence of Ca^{2+} however, had a synergistic effect on the binding of Cu(II) where the binding of Cu(II) increased as the concentration of the Ca^{2+} increased[10].

CHAPTER IV

CONCLUSIONS

A hydrothermal synthesis method was employed for the synthesis of Fe_7S_8 which produced a mixture of 90% Fe_7S_8 and 10% Fe_3S_4 with particle sizes of 23.3 nm and 18.7 nm, respectively. Since the main component of the mixture was Fe_7S_8, the results correspond to the pyrrhotite phase. A hydrothermal synthesis method was also used synthesize ZnS which yielded a particle size of 7.0 ± 0.22 nm. Furthermore, TiS_2 was synthesized via a reflux method at 300˚C and produced particle sizes of 8.03 ± 0.98 nm.

pH profile studies were conducted to determine the optimal pH for adsorption which showed that the sorption of Pb(II) with Fe_7S_8 was pH dependent in which the binding increased as the pH increased whereas Cu(II) was pH independent with 100% throughout all pH's tested. The sorption of both metals with ZnS in ambient light showed no effect on the binding as the pH increased. On the other hand, the sorption of both metal ions with TiS_2 were pH dependent and the binding decreased as the pH increased. Furthermore, due to the photoactivity of ZnS, UV-light and "Dark" pH profile assays were conducted and it was determined that UV-light had no effect on the sorption of either Pb(II) or Cu(II). The absence of light "Dark" however had an effect on the binding of Pb(II); the percent binding decreased as the was pH increased. The sorption of Cu(II) in the absence of light showed no effect.

Time dependency studies revealed that the sorption of Pb(II) and Cu(II) with Fe_7S_8, ZnS in the absence of light, and TiS_2 were time dependent. The maximum binding for Pb(II) with

Fe_7S_8 and TiS_2 occurred with 240 min (4h) of contact time, whereas the sorption for Cu(II) occurred with 60 min of contact time. The sorption of Pb(II) with ZnS in the dark showed a maximum binding of 85% with 60 min of contact time. The sorption of both ions with ZnS in ambient light showed no effect with contact time and a maximum binding occurred within the first 5 min of contact time.

In addition, the thermodynamic studies shown for the most part the reactions were endothermic. The only material that showed an exothermic reaction was the binding of the Cu(II) to the TiS_2 nanomaterial. Further thermodynamic data showed the binding of Pb(II) to the Fe_7S_8 nanomaterial was chemisorption, to the ZnS (light)was physisorption, ZnS (dark) was ion exchange, and TiS_2 chemisorption. Cu(II) ions bound to the Fe_7S_8 through chemisorption, ZnS was through physisorption, and the TiS_2 was through ion exchange mechanisms.

The transition metal sulfide nanomaterials tested proved to be successful in the removal of both Pb(II) and Cu(II). The sorption of Pb(II) with the materials followed the same trend in which the capacity increased with an increase in temperature. Similarly, the sorption of Cu(II) with the transition metal sulfides appeared to follow the same trend as the binding of Pb(II) except with TiS_2 in which the binding capacity decreased as the temperature increased. Comparing the results, in mmol/g, Cu(II) binding is preferred over Pb(II) binding to all nano-metal sulfides since at all temperatures the capacity for Cu(II) is higher than Pb(II).

The presence of individual interfering cations for the sorption of Pb(II) with the nano-metal sulfides generally showed little to no effect on the binding. In the presence of higher concentrations of Na^+, the sorption of Pb(II) with Fe_7S_8 showed a synergistic effect in which the percent binding increased. On the other hand, the sorption of Cu(II) with the transition metal sulfides showed to have an antagonist effect as the concentrations of the cations increased. The

combination of all cations on the sorption of Pb(II) with Fe_7S_8 showed no effect whereas with ZnS showed a synergistic effect in which the binding increased steadily. The sorption of Pb(II) with TiS_2 in the presence of all cations caused no effect on the binding except in the presence of 3 ppm and 300 ppm which increased the binding by approximately 20%. On the other hand, the sorption of Cu(II) with the metal sulfides in the presence of all cations generally showed an antagonistic effect after a concentration of 3 ppm except on the sorption with TiS_2 where no effect was observed as the concentrations increased.

REFERENCES

[1] Hoekstra, A. Y., and M. M. Mekonnen. “The Monthly Blue Water Footprint Compared to Blue Water Availabillity for the Worlds Major River Basins.” *Unesco-Ihe*, no. Value of Water Research Report Series No.53, 2011, p. 78.

[2] Gaetke, Lisa M., and Ching Kuang Chow. “Copper Toxicity, Oxidative Stress, and Antioxidant Nutrients.” *Toxicology*, vol. 189, no. 1–2, 2003, pp. 147–163, doi:10.1016/S0300-483X(03)00159-8.

[3] Gordon, B., et al. “WHO Guidelines for Drinking-Water Quality.” *WHO Chronicle*, vol. 38, no. 3, 2008, p. 564, doi:10.1016/S1462-0758(00)00006-6.

[4] “National Primary Drinking Water Regulations.” EPA, Environmental Protection Agency, 11 July 2017, www.epa.gov/ground-water-and-drinking-water/national-primary-drinking-water-regulations.

[5] Needleman, Herbert. “Lead Poisoning.” *Annual Review of Medicine*, vol. 55, no. 1, 2004, pp. 209–222, doi:10.1146/annurev.med.55.091902.103653.

[6] Tong, S., et al. “Environmental Lead Exposure: A Public Health Problem of Global Dimensions.” *Bulletin of the World Health Organization*, vol. 78, no. 9, 2000, pp. 1068–1077, doi:10.1590/S0042-96862000000900003.

[7] WHO. “Lead in Drinking-Water.” *Guidelines for Drinking-Water Quality*, vol. 9, 2003, p., doi:10.1155/2013/959637.

[8] Wu, Wenqin, et al. “Highly Efficient Removal of Cu(II) from Aqueous Solution by Using Graphene Oxide.” *Water, Air, & Soil Pollution*, vol. 224, no. 1, 2013, p. 1372, doi:10.1007/s11270-012-1372-5.

[9] Georgopoulos, Panos G., et al. “Assessment of Human Exposure to Copper: A Case Study Using the NHEXAS Database.” *Journal of Exposure Science & Environmental Epidemiology*, vol. 16, no. 5, 2006, pp. 397–409, doi:10.1038/sj.jea.7500462

[10] Tamez, Carlos, et al. “Removal of Cu (II) and Pb (II) from Aqueous Solution Using Engineered Iron Oxide Nanoparticles.” *Microchemical Journal*, vol. 125, Elsevier B.V., 2016, pp. 97–104, doi:10.1016/j.microc.2015.10.028.

[11] Liu, Yan, et al. “Synthesis of Magnetic Polyaniline/graphene Oxide Composites and Their Application in the Efficient Removal of Cu(II) from Aqueous Solutions.” *Journal of Environmental Chemical Engineering*, vol. 4, no. 1, Elsevier B.V., 2016, pp. 825–834, doi:10.1016/j.jece.2015.12.023.

[12] Ahmad, Anees, et al. “Removal of Cu(II) and Pb(II) Ions from Aqueous Solutions by Adsorption on Sawdust of Meranti Wood.” *Desalination*, vol. 247, no. 1–3, Elsevier B.V., 2009, pp. 636–646, doi:10.1016/j.desal.

[13] Fu, Fenglian, and Qi Wang. “Removal of Heavy Metal Ions from Wastewaters: A Review.” *Journal of Environmental Management*, vol. 92, no. 3, Elsevier Ltd, 2011, pp. 407–418, doi:10.1016/j.jenvman.2010.11.011.

[14] Farghali, A. A., et al. “Adsorption of Pb(II) Ions from Aqueous Solutions Using Copper Oxide Nanostructures.” *Beni-Suef University Journal of Basic and Applied Sciences*, vol. 2, no. 2, Elsevier Ltd, 2013, pp. 61–71, doi:10.1016/j.bjbas.2013.01.001.

[15] Sitko, Rafal, et al. “Adsorption of Divalent Metal Ions from Aqueous Solutions Using Graphene Oxide.” *Dalton Transactions*, vol. 42, no. 16, 2013, p. 5682, doi:10.1039/c3dt33097d.

[16] Wang, Xiangxue, et al. “Application of Graphene Oxides for the Removal of Pb(II) Ions from Aqueous Solutions: Experimental and DFT Calculation.” *Journal of Molecular Liquids*, vol. 211, Elsevier B.V., 2015, pp. 957–964, doi:10.1016/j.molliq.2015.08.020.

[17] Mahdavi, Shahriar, et al. “Removal of Heavy Metals from Aqueous Solutions Using Fe3O4, ZnO, and CuO Nanoparticles.” *Journal of Nanoparticle Research*, vol. 14, no. 8, 2012, p. 846, doi:10.1007/s11051-012-0846-0.

[18] Wang, Hongyu, et al. “Removal of Pb(II), Cu(II), and Cd(II) from Aqueous Solutions by Biochar Derived from KMnO4 Treated Hickory Wood.” *Bioresource Technology*, vol. 197, Elsevier Ltd, 2015, pp. 356–362, doi:10.1016/j.biortech.2015.08.132.

[19] Azzam, Ahmed M., et al. “Removal of Pb, Cd, Cu and Ni from Aqueous Solution Using Nano Scale Zero Valent Iron Particles.” *Journal of Environmental Chemical Engineering*, vol. 4, no. 2, Elsevier B.V., 2016, pp. 2196–2206, doi:10.1016/j.jece.2016.03.048.

[20] Cantu, Jesus, et al. “Removal of Arsenic from Water Using Synthetic Fe7S8 Nanoparticles.” *Chemical Engineering Journal*, vol. 290, Elsevier B.V., 2016, pp. 428–437, doi:10.1016/j.cej.2016.01.053.

[21] Hoa, Tran Thi Quynh, et al. “Preparation of ZnS nanoparticles by hydrothermal method.” Journal of Physics: Conference Series, vol. 187, Jan. 2009, p. 012081., doi:10.1088/1742-6596/187/1/012081.

[22] Prabakar, Sujay, et al. “Liquid-Phase Synthesis of Flower-like and Flake-like Titanium Disulfide Nanostructures.” *Chemistry of Materials*, vol. 21, no. 8, 2009, pp. 1725–1730, doi:10.1021/cm900110h.

[23] M. Tokonami, et al. “Crystal structure of a monoclinic pyrrhotite (Fe7S8).” *Am. Mineral,* vol 57, 1972, pp. 1066-1080.

[24] B.J. Skinner, et al. “Greigite, the thio-spinel of iron: a new mineral.” *Am. Mineral,* vol. 49, 1964, pp. 543–555.

[25] Biswas, Subhajit, et al. “Fabrication of ZnS nanoparticles and nanorods with cubic and hexagonal crystal structures: a simple solvothermal approach.” *Nanotechnology*, vol. 19, 2008, p. 045710.

[26] Fan, Qiaohui, et al. “Adsorption of Pb(II) on Palygorskite from Aqueous Solution: Effects of pH, Ionic Strength and Temperature.” *Applied Clay Science*, vol. 45, no. 3, Elsevier B.V., 2009, pp. 111–116, doi:10.1016/j.clay.2009.04.009.

[27] Gadde, Rao, et al. “Studies of Heavy Metal Adsorption by Hydrous Iron and Manganese Oxides.” *Analytical chemistry*. Vol. 46, no. 13, 1974, pp. 2022–2026.

[28] Fouladgar, Malihe, et al. “Single and Binary Adsorption of Nickel and Copper from Aqueous Solutions by ??-Alumina Nanoparticles: Equilibrium and Kinetic Modeling.” *Journal of Molecular Liquids*, vol. 211, Elsevier B.V., 2015, pp. 1060–1073, doi:10.1016/j.molliq.2015.08.029.

[29] Chen, Yen Hua, and Fu An Li. “Kinetic Study on Removal of copper(II) Using Goethite and Hematite Nano-Photocatalysts.” *Journal of Colloid and Interface Science*, vol. 347, no. 2, Elsevier Inc., 2010, pp. 277–281, doi:10.1016/j.jcis.2010.03.050.

[30] Gupta, V. K., and A. Rastogi. “Biosorption of Lead from Aqueous Solutions by Green Algae Spirogyra Species: Kinetics and Equilibrium Studies.” *Journal of Hazardous Materials*, vol. 152, no. 1, 2008, pp. 407–414, doi:10.1016/j.jhazmat.2007.07.028.

[31] Zou, Weihua, et al. “Kinetic Study of Adsorption of Cu(II) and Pb(II) from Aqueous Solutions Using Manganese Oxide Coated Zeolite in Batch Mode.” *Colloids and Surfaces A: Physicochemical and Engineering Aspects*, vol. 279, no. 1–3, 2006, pp. 238–246, doi:10.1016/j.colsurfa.2006.01.008.

[32] Castaldi, Paola, et al. “Copper(II) and lead(II) Removal from Aqueous Solution by Water Treatment Residues.” *Journal of Hazardous Materials*, vol. 283, Elsevier B.V., 2015, pp. 140–147, doi:10.1016/j.jhazmat.2014.09.019.

[33] Hua, Ming, et al. “Heavy Metal Removal from Water/wastewater by Nanosized Metal Oxides: A Review.” *Journal of Hazardous Materials*, vol. 211–212, 2012, pp. 317–331, doi:10.1016/j.jhazmat.2011.10.016.

[34] Nadaroglu, Hayrunnisa, et al. “Removal of Copper from Aqueous Solution Using Red Mud.” *Desalination*, vol. 251, no. 1–3, Elsevier B.V., 2010, pp. 90–95, doi:10.1016/j.desal.2009.09.138.

[35] Al-Anber, Mohammed. “Thermodynamics Approach in the Adsorption of Heavy Metals.” *Intech*, 2011.

[36] Han, Runping, et al. “Removal of copper(II) and lead(II) from Aqueous Solution by Manganese Oxide Coated Sand. II. Equilibrium Study and Competitive Adsorption.” *Journal of Hazardous Materials*, vol. 137, no. 1, 2006, pp. 480–488, doi:10.1016/j.jhazmat.2006.02.018.

[37] Ben-Ali, Samia, et al. “Characterization and Adsorption Capacity of Raw Pomegranate Peel Biosorbent for Copper Removal.” *Journal of Cleaner Production*, vol. 142, Elsevier Ltd, 2017, pp. 3809–3821, doi:10.1016/j.jclepro.2016.10.081.

BIOGRAPHICAL SKETCH

Jesus Manuel Cantu was born in 1995 in Waukegan, Illinois. He grew up in Roma, Texas and graduated high school in 2013. He attended South Texas College while in high school and earned an associate of science in Biology in 2013. He then attended the University of Texas Rio Grande Valley where he earned a bachelor's of science in Chemistry. He began the M.S. in chemistry program on January of 2016 where he worked as a graduate assistant throughout the duration of the program. Mr. Cantu graduated with his M.S. in Chemistry degree in December of 2017.

Mr. Cantu can be contacted at jcantu1249@gmail.com.